

# Spatially Coupled PLDPC-Hadamard Convolutional Codes

Peng W. Zhang, Francis C.M. Lau, *Fellow, IEEE*, and Chiu-W. Sham, *Senior  
Member, IEEE*

## Abstract

In this paper, we propose a new type of ultimate-Shannon-limit-approaching codes called spatially coupled protograph-based low-density parity-check Hadamard convolutional codes (SC-PLDPCH-CCs), which are constructed by spatially coupling PLDPC-Hadamard block codes. We also develop an efficient decoding algorithm that combines pipeline decoding and layered scheduling for the decoding of SC-PLDPCH-CCs. To estimate the decoding thresholds of SC-PLDPCH-CCs, we first propose a layered protograph extrinsic information transfer (PEXIT) algorithm to evaluate the thresholds of spatially coupled PLDPC-Hadamard terminated codes (SC-PLDPCH-TDCs) with a moderate coupling length. With the use of the proposed layered PEXIT method, we develop a genetic algorithm to look for good SC-PLDPCH-TDCs in a systematic way. Subsequently, we extend the coupling length of these SC-PLDPCH-TDCs with good thresholds to form good SC-PLDPCH-CCs. Based on the same set of split protomatrices, we regard the threshold of SC-PLDPCH-TDC as the proxy of SC-PLDPCH-CC when the SC-PLDPCH-TDC with long coupling length has almost the same code rate as the SC-PLDPCH-CC. Results show that our optimized SC-PLDPCH-CCs can achieve comparable thresholds to the block code counterparts. Simulations also illustrate the superiority of the SC-PLDPCH-CCs over the block code counterparts in terms of error performance. Moreover, for the rate-0.00295 SC-PLDPCH-CC, a BER of  $10^{-7}$  is achieved at  $E_b/N_0 = -1.45$  dB, which is only 0.14 dB from the ultimate Shannon limit.

## Index Terms

Protograph LDPC code, PLDPC-Hadamard code, PEXIT algorithm, spatially coupled PLDPC codes, spatially coupled PLDPC Hadamard codes, ultimate Shannon limit.

P.W. Zhang and F.C.M. Lau are with the Future Wireless Networks and IoT Focusing Area, Department of Electronic and Information Engineering, The Hong Kong Polytechnic University, Hong Kong (e-mail: pengwei.zhang@connect.polyu.hk and francis-cm.lau@polyu.edu.hk).

C.-W. Sham is with the Department of Computer Science, The University of Auckland, New Zealand (e-mail: b.sham@auckland.ac.nz).

## I. INTRODUCTION

Low-density parity-check (LDPC) codes were first proposed in 1963 [1], whose sparse parity-check matrix containing “0” and “1” is randomly constructed, and can be graphically represented by a Tanner graph [2]. A Tanner graph consists of check nodes (CNs), variable nodes (VNs) and the connections between CNs and VNs. When all VN degrees are the same and all CN degrees are identical, the corresponding code is a regular LDPC code; otherwise it is an irregular LDPC code. After receiving the channel observations, extrinsic information along the connections is iteratively exchanged and calculated at check node processors and variable node processors so as to realize belief propagation (BP) decoding. In [3], a density evolution method has been proposed to evaluate the probability density function (PDF) of the extrinsic information and hence to optimize the degree distributions of LDPC codes. Subsequently in [4], an extrinsic information transfer (EXIT) chart technique has been proposed to optimize LDPC codes by calculating the mutual information of the extrinsic information. Through both methods, good-performing LDPC codes have been constructed to work close to the Shannon limit under binary erasure channels (BECs), binary symmetric channels (BSCs) and additive-white-Gaussian-noise (AWGN) channels [3], [4], [5]. LDPC codes are also widely used in modern digital communication systems such as 3G/4G/5G, WiFi, digital video broadcasting and satellite communications.

Yet, most LDPC codes are designed to achieve good decoding performance at a bit-energy-to-noise-power-spectral-density ratio ( $E_b/N_0$ ) greater than 0 dB. To approach the ultimate Shannon limit, i.e.,  $E_b/N_0 = -1.59$  dB [6], other low-rate codes should be designed. Potential application scenarios of such codes include multiple access wireless systems (e.g., interleaved-division multiple-access [7], [8] with a huge number of non-orthogonal users), and deep space communications. In [9] and [10], very low-rate turbo Hadamard codes and zigzag Hadamard codes have been proposed. However, their decoders require the use of serial decoding [11], [12], [13] and cannot make use of parallel decoding as in LDPC decoders. The error performances of turbo Hadamard codes and zigzag Hadamard codes are also not as good as those of the LDPC-Hadamard codes that are subsequently proposed [14].

In the Tanner graph of an LDPC code, the edges connected to a VN form a repeat code, whereas the edges connected to a CN form a single-parity-check (SPC) code. When the repeat codes and/or SPC codes are replaced with other block codes, a Tanner graph of a generalized LDPC is formed. By replacing SPC codes with Hadamard codes, LDPC-Hadamard codes have

been proposed and their degree distributions have been optimized with the EXIT chart method [14]. The LDPC-Hadamard codes not only have thresholds lower than  $-1.34$  dB, but also achieve excellent decoding performance at a  $E_b/N_0$  lower than  $-1.17$  dB. On the other hand, the EXIT chart method cannot effectively analyze degree distributions containing degree-1 and/or punctured VNs. The parity-check matrix derived by the progressive-edge-growth (PEG) method [15] according to the degree distributions does not contain any structure and therefore does not facilitate linear encoding and parallel decoding.

To solve the above problems, a class of structured LDPC-Hadamard codes called protograph-based LDPC-Hadamard (PLDPC-Hadamard) codes have been proposed from the perspective of protographs [16], [17]. Protograph-based LDPC (PLDPC) codes can be described by a small protomatrix or protograph [18]. Using the copy-and-permute operations to lift the protomatrix or protograph, the derived matrix or lifted graph can easily have a quasi-cyclic (QC) structure which is conducive to the hardware implementations of encoders and decoders [19]. PLDPC-Hadamard codes [16], [17] also inherit such advantages from PLDPC codes. By adding an appropriate amount of degree-1 Hadamard variable nodes (D1H-VNs) to the check nodes in the protograph of a PLDPC code, the SPC constraints are converted into Hadamard constraints and the protograph of a PLDPC-Hadamard code is obtained. The protograph-based EXIT (PEXIT) chart method for PLDPC codes [20] has further been modified for analyzing PLDPC-Hadamard codes [16], [17]. The modified method not only can produce multiple extrinsic mutual information from the symbol-by-symbol maximum-a-posteriori-probability (symbol-MAP) Hadamard decoder, but also is applicable to analyzing protographs with degree-1 and/or punctured VNs. The structured PLDPC-Hadamard codes can achieve good thresholds and comparable error performance as the traditional LDPC-Hadamard codes. In [21], a layered decoding algorithm has been proposed to double the convergence rate compared with standard decoding.

While PLDPC-Hadamard codes are already working very close to the ultimate Shannon limit, further improvement is possible. Recall that LDPC convolutional codes (LDPC-CCs) can achieve convolutional gains over their block-code counterparts by applying windowed decoding [22]. LDPC-CCs were first proposed in [23] and characterized by the degree distributions of the underlying LDPC block codes (LDPC-BCs). In addition, spatially coupled LDPC (SC-LDPC) codes are constructed by coupling a number of LDPC-BCs. As the number of coupled LDPC-BCs tends to infinity, spatially coupled LDPC convolutional codes (SC-LDPC-CCs) are obtained. In [24] and [25], SC-LDPC-CCs have been shown to achieve capacity over binary

memoryless symmetric channels under belief propagation (BP) decoding. In [26], SC-LDPC-CCs have been constructed from the perspective of protographs, namely SC-PLDPC-CCs. Through the edge-spreading procedure on protomatrix, the threshold, convergence behavior and error performance of SC-PLDPC ensembles have also been systematically investigated. Based on the aforementioned results, spatially coupled PLDPC-Hadamard convolutional codes (SC-PLDPCH-CCs), which are to be investigated in this paper, have the potential to provide extra gains over their block-code counterparts. A genetic algorithm will also be proposed to optimize the design of SC-PLDPCH-CCs.

Genetic algorithm (GA) is an optimization algorithm that simulates the evolution of nature, and is widely used in music generation, genetic synthesis and VLSI technology [27]. In the arena of channel codes, GA has been applied to adjust the code rate of turbo codes without puncturing [28]; to construct polar codes that can reduce the decoding complexity while maintaining the same decoding performance [29]; together with bit-error-rate (BER) simulations to optimize error performance of short length LDPC codes over both AWGN and Rayleigh fading channels [30]; together with density evolution to optimize the degree distributions of the SC-LDPC codes over BEC channels [31].

In this paper we propose a new type of ultimate-Shannon-limit-approaching codes, namely spatially coupled PLDPC-Hadamard convolutional codes (SC-PLDPCH-CCs), and have conducted an in-depth investigation into the proposed codes. We summarize the main contributions as follows.

- 1) We propose a new type of ultimate-Shannon-limit-approaching codes, namely spatially coupled PLDPC-Hadamard convolutional codes (SC-PLDPCH-CCs), which are constructed by spatially coupling PLDPC-Hadamard block codes.
- 2) We describe the encoding method of SC-PLDPCH-CCs. We also develop an efficient decoding algorithm, i.e., a pipeline decoding strategy combined with layered scheduling, for the decoding of SC-PLDPCH-CCs.
- 3) Using the original PEXIT method in [16], [17], we show that the thresholds of different spatially coupled PLDPC-Hadamard terminated codes (SC-PLDPCH-TDCs) are distinguishable and improves as the coupling length increases. To improve the convergence rate of the original PEXIT method, we propose a layered PEXIT chart algorithm to efficiently evaluate the threshold of SC-PLDPCH-TDCs with a given coupling length. The thresholds of SC-PLDPCH-TDCs with large coupling length are then used as estimates for thresholds

of SC-PLDPCH-CCs.

- 4) We propose a genetic algorithm (GA) to systematically search for SC-PLDPCH-TDCs having good thresholds. Based on the same set of split protomatrices for good SC-PLDPCH-TDCs, we extend the coupling length to construct the convolutional codes, i.e., SC-PLDPCH-CCs.
- 5) We have found SC-PLDPCH-CCs with comparable thresholds to the underlying PLDPC-Hadamard block codes. Simulation results show that SC-PLDPCH-CCs outperform their PLDPC-Hadamard block code counterparts in terms of bit error performance. For the rate-0.00295 SC-PLDPCH-CC, a BER of  $10^{-7}$  is achieved at  $E_b/N_0 = -1.45$  dB.

The remainder of the paper is organized as follows. Section II briefly reviews the structures of the related LDPC block codes and spatially coupled LDPC codes. Section III introduces the structure and encoding process of SC-PLDPCH-CCs. It also describes a pipeline decoding strategy combined with layered scheduling for decoding SC-PLDPCH-CCs. Moreover, a layered PEXIT chart method is proposed to evaluate the threshold of SC-PLDPCH-TDCs/SC-PLDPCH-CCs efficiently and a GA is proposed to optimize protomatrices for SC-PLDPCH-TDCs/SC-PLDPCH-CCs. Section IV presents the thresholds and optimized protomatrices of SC-PLDPCH-CCs with different code rates. It also compares the simulated BER results of the SC-PLDPCH-CCs with those of the underlying PLDPCH-BCs. Finally, Section V presents some concluding remarks.

## II. BACKGROUND

### A. LDPC and PLDPC Block Codes

An LDPC block code can be represented by a  $M \times N$  parity-check matrix  $\mathbf{H} = \{h(i, j) : i = 1, 2, \dots, M; j = 1, 2, \dots, N\}$ , where the entries  $h(i, j)$  are either “0” or “1” and the proportion of “1”s in  $\mathbf{H}$  is very small. Moreover, any LDPC codeword  $\mathbf{c}$ , which has a length of  $N$ , has to fulfill  $\mathbf{c}\mathbf{H}^T = \mathbf{0}$ , where  $(\cdot)^T$  is transpose operator and  $\mathbf{0}$  is the length- $M$  zero vector. For a full-rank  $\mathbf{H}$ , the code rate of the LDPC block code equals  $R_{\text{LDPC-BC}} = 1 - M/N$ . If all column weights are the same and all row weights are the same,  $\mathbf{H}$  corresponds to a regular LDPC code; otherwise, it corresponds to an irregular code. An LDPC code can also be represented by a Tanner graph [2]. Each row of  $\mathbf{H}$  corresponds to a check node (CN) with a SPC constraint, i.e., a SPC-CN; each column of  $\mathbf{H}$  corresponds to a variable node (VN); and the entry  $h(i, j) = 1/0$  corresponds to one/no edge between the  $i$ -th SPC-CN and the  $j$ -th VN.

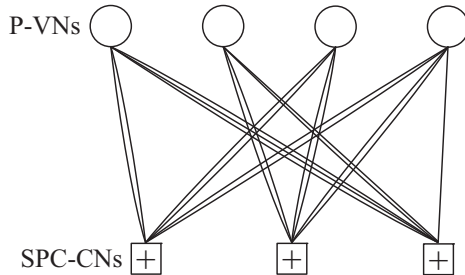


Fig. 1. A protograph consisting of  $m = 3$  SPC-CNs and  $n = 4$  P-VNs. The corresponding protomatrix is given in (1).

When an LDPC code is characterized by and constructed from a small protograph or protomatrix [18], it is called a protograph-based LDPC (PLDPC) code. A protograph consists of a set of  $m$  SPC-CNs, a set of  $n$  ( $n > m$ ) protograph variable nodes (P-VNs), and a set of edges connecting the SPC-CNs to the P-VNs. Moreover, parallel edges are allowed. Fig. 1 illustrates a protograph that contains  $m = 3$  SPC-CNs (each represented by a box with a plus symbol inside), and  $n = 4$  P-VNs (each represented by a circle). The corresponding protomatrix, which has a size of  $m \times n (= 3 \times 4)$ , is given by

$$\mathbf{B} = \begin{bmatrix} 2 & 0 & 2 & 2 \\ 0 & 2 & 2 & 2 \\ 3 & 2 & 0 & 1 \end{bmatrix}. \quad (1)$$

Each row in  $\mathbf{B}$  corresponds to a SPC-CN; each column corresponds to a P-VN; and the  $(i, j)$ -th entry, denoted by  $b(i, j)$ , corresponds to the number of edges connecting the  $i$ -th SPC-CN and the  $j$ -th P-VN. Since parallel edges are allowed in the protograph, the entries in the protomatrix can be greater than 1. Based on  $m$  and  $n$ , the code rate of a PLDPC block code can be computed using

$$R_{\text{PLDPC-BC}} = 1 - \frac{m}{n}. \quad (2)$$

A two-step lifting method can be used to lift the protomatrix and hence to construct a parity-check matrix [32]. We denote the first and second lifting factors by  $z_1$  and  $z_2$ , respectively. The first lifting procedure aims to eliminate the entries greater than 1 in the protomatrix. Thus for an entry  $b(i, j) > 0$ , it is replaced with a summation of  $b(i, j)$  different  $z_1 \times z_1$  permutation matrices; for an entry  $b(i, j) = 0$ , it is replaced with the  $z_1 \times z_1$  zero matrix. After the first lifting, all entries in the lifted matrix is either “0” or “1”. The second lifting procedure aims

to construct a parity-check matrix with a quasi-cyclic (QC) structure so as to simplify encoder and decoder designs. Thus for an entry “1” in the lifted matrix, it is replaced with a circulant permutation matrix (CPM) of size  $z_2 \times z_2$ ; for an entry “0”, it is replaced with the  $z_2 \times z_2$  zero matrix. The two-step lifting method not only makes the derived matrix possessing QC structure, but also keeps both degree distributions and code rate unchanged.

### B. LDPC-Hadamard and PLDPC-Hadamard Block Codes

A Hadamard code with an order  $r$  has a code length of  $q = 2^r$  and can be obtained by a Hadamard matrix  $\mathbf{H}_q$  of size  $q \times q$ .  $\mathbf{H}_q$  can be recursively generated using [9], [14]

$$\pm \mathbf{H}_q = \pm \{\mathbf{h}_j\} = \begin{bmatrix} \pm \mathbf{H}_{q/2} & \pm \mathbf{H}_{q/2} \\ \pm \mathbf{H}_{q/2} & \mp \mathbf{H}_{q/2} \end{bmatrix} \quad (3)$$

where  $\pm \mathbf{H}_1 = [\pm 1]$ ;  $\pm \mathbf{h}_j = [\pm h_{0,j} \ \pm h_{1,j} \ \cdots \ \pm h_{2^{r-1},j}]^T$  ( $j = 0, 1, \dots, q-1$ ) represents the  $j$ -th column of  $\pm \mathbf{H}_q$  and is a Hadamard codeword. Fig. 2 shows the Hadamard matrix  $\pm \mathbf{H}_{16}$ , i.e., when  $r = 4$ . Suppose  $+1$  is mapped to bit “0” and  $-1$  to bit “1”. It has been shown that when the Hadamard order  $r$  is an even number, the 0th, 1st, 2nd,  $\dots$ ,  $2^{k-1}$ -th,  $\dots$ ,  $2^{r-1}$ -th, and  $(2^r - 1)$ -th code bits (total  $r + 2$  bits) in each codeword  $\pm \mathbf{h}_j$  satisfy the SPC constraint together, i.e., [14], [16], [17]

$$[\pm h_{0,j} \oplus \pm h_{1,j} \oplus \cdots \oplus \pm h_{2^{k-1},j} \oplus \cdots \oplus \pm h_{2^{r-1},j}] \oplus \pm h_{2^r-1,j} = 0, \quad (4)$$

where the symbol  $\oplus$  represents the XOR operator. Fig. 2 also illustrates  $\pm h_{0,j} \oplus \pm h_{1,j} \oplus \pm h_{2,j} \oplus \pm h_{4,j} \oplus \pm h_{8,j} \oplus \pm h_{15,j} = 0 \ \forall j$ .

For an LDPC block code, each VN represents a repeat code, meaning that all its connections should have the same bit value; whereas each SPC-CN requires all its connecting edges fulfilling the SPC constraint together. When the SPC codes of an LDPC code are replaced with Hadamard block codes with additional Hadamard parity-check bits, i.e., the SPC-CN's are replaced with Hadamard check nodes (H-CN's) with additional Hadamard parity-check bits, a LDPC-Hadamard block code is formed [14].

LDPC-Hadamard codes can be constructed by lifting protographs in which the SPC-CN's have been replaced with H-CN's and additional parity-check bits. Such LDPC-Hadamard block codes are called protograph-based PLDPC-Hadamard block codes (PLDPCH-BCs) [16], [17].







where each  $\mathbf{H}_i(t)$  ( $i = 0, 1, \dots, m_s$ ) is a  $M \times N$  component matrix,  $t$  denotes the time index, and  $m_s$  is the syndrome former memory. Each codeword  $\mathbf{c}$  should satisfy  $\mathbf{c}\mathbf{H}_{CC}^T = \mathbf{0}$ , where  $\mathbf{0}$  is a semi-infinite zero vector.

2) *Spatially coupled PLDPC codes*: Spatially coupled PLDPC codes are constructed based on underlying PLDPC block codes. We denote  $W$  as the coupling width (equivalent to the aforementioned syndrome former memory  $m_s$ ) and  $L$  as the coupling length. Based on the  $m \times n$  protomatrix  $\mathbf{B}$  of an underlying PLDPC code, an edge-spreading procedure can be first used to obtain  $W + 1$  split protomatrices  $\mathbf{B}_i$  ( $i = 0, 1, \dots, W$ ) under the constraint  $\mathbf{B} = \sum_{i=0}^W \mathbf{B}_i$ . Then  $L$  sets of such protomatrices are coupled to construct a spatially coupled PLDPC (SC-PLDPC) code [26]. Depending on how the coupling ends, three types of SC-PLDPC codes, namely SC-PLDPC terminated code (SC-PLDPC-TDC), SC-PLDPC tail-biting code (SC-PLDPC-TBC) and SC-PLDPC convolutional codes (SC-PLDPC-CC), are formed.

When the  $L$  sets of protomatrices are coupled and then directly terminated, the resultant protomatrix is given by

$$\mathbf{B}_{\text{SC-PLDPC-TDC}} = \left[ \begin{array}{cccc} \overbrace{\mathbf{B}_0}^{nL} & & & \\ \mathbf{B}_1 & \mathbf{B}_0 & & \\ \vdots & \mathbf{B}_1 & \ddots & \\ \mathbf{B}_W & \vdots & \ddots & \mathbf{B}_0 \\ & \mathbf{B}_W & \ddots & \mathbf{B}_1 \\ & & \ddots & \vdots \\ & & & \mathbf{B}_W \end{array} \right] \left. \vphantom{\begin{array}{c} \mathbf{B}_0 \\ \mathbf{B}_1 \\ \vdots \\ \mathbf{B}_W \\ \mathbf{B}_W \end{array}} \right\} m(L+W). \quad (7)$$

Such code is called a SC-PLDPC-TDC. The code rate equals

$$\begin{aligned} R_{\text{SC-PLDPC-TDC}} &= \frac{nL - m(L + W)}{nL} \\ &= 1 - \frac{L + W}{L} (1 - R_{\text{PLDPC-BC}}), \end{aligned} \quad (8)$$

where  $R_{\text{PLDPC-BC}} = 1 - \frac{m}{n}$  is the code rate of its underlying block code.

Example: We make use of the protomatrix (1) to construct the protomatrix of a SC-PLDPC-TDC. We assume a coupling width  $W = 1$ . Hence we split  $\mathbf{B}$  into  $\mathbf{B}_0$  and  $\mathbf{B}_1$  under the constraint

$\mathbf{B} = \mathbf{B}_0 + \mathbf{B}_1$ , and obtain

$$\mathbf{B}_0 = \begin{bmatrix} 1 & 0 & 0 & 2 \\ 0 & 1 & 1 & 1 \\ 1 & 2 & 0 & 1 \end{bmatrix} \quad (9)$$

and

$$\mathbf{B}_1 = \begin{bmatrix} 1 & 0 & 2 & 0 \\ 0 & 1 & 1 & 1 \\ 2 & 0 & 0 & 0 \end{bmatrix}. \quad (10)$$

Assuming a coupling length  $L = 3$ , we can construct the protomatrix of a SC-PLDPC-TDC as

$$\mathbf{B}_{\text{TDC}, W=1, L=3} = \begin{bmatrix} \mathbf{B}_0 & & & \\ \mathbf{B}_1 & \mathbf{B}_0 & & \\ & \mathbf{B}_1 & \mathbf{B}_0 & \\ & & & \mathbf{B}_1 \end{bmatrix}. \quad (11)$$

The protograph of the above SC-PLDPC-TDC is shown in Fig. 4, which is formed by coupling  $L = 3$  PLDPC-BC protographs. The blue edges (connecting P-VNs and SPC-CN) correspond to  $\mathbf{B}_0$  (9) while the red ones correspond to  $\mathbf{B}_1$  (10). According to edge-spreading operations, the edges from the P-VNs at time  $t$  will be spread to connect the SPC-CN at time  $t + 1, t + 2, \dots, t + W$  in addition to the SPC-CN at time  $t$ . Hence in Fig. 4, the P-VNs at time  $t = 1$  connect SPC-CN at time  $t = 1$  and  $t = 2$  as  $W = 1$ , and P-VNs at time  $t = 2$  connect SPC-CN at time  $t = 2$  and  $t = 3$ .

In Fig. 5, we illustrate another example where  $W = 2$  and  $L = 4$ . The  $\mathbf{B}$  in (1) is split into

$$\mathbf{B}_0 = \begin{bmatrix} 1 & 0 & 0 & 1 \\ 0 & 0 & 1 & 1 \\ 0 & 1 & 0 & 0 \end{bmatrix}, \quad (12)$$

$$\mathbf{B}_1 = \begin{bmatrix} 1 & 0 & 1 & 0 \\ 0 & 1 & 1 & 1 \\ 2 & 0 & 0 & 0 \end{bmatrix} \quad (13)$$



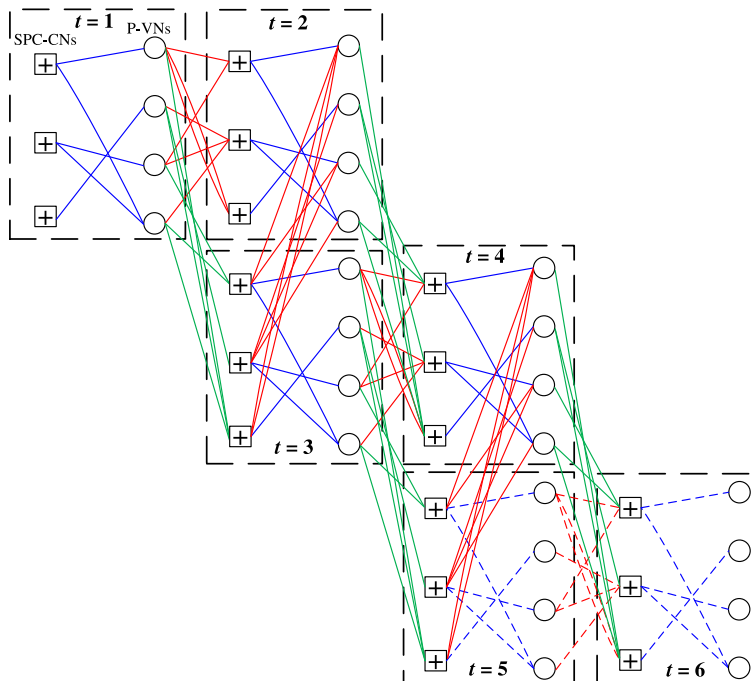


Fig. 5. The protograph of a SC-PLDPC-TDC with  $W = 2$  and  $L = 4$ . The P-VNs corresponding to  $t = 5$  and  $t = 6$  and their associated connections do not exist.

the corresponding code is called SC-PLDPC-TBC, whose protomatrix can be written as

$$\mathbf{B}_{\text{SC-PLDPC-TBC}} = \overbrace{\left[ \begin{array}{cccc} B_0 & & B_W & \cdots & B_1 \\ B_1 & B_0 & & & \vdots \\ \vdots & B_1 & B_0 & & B_W \\ B_W & \vdots & B_1 & \ddots & \\ & B_W & \vdots & \ddots & B_0 \\ & & B_W & \ddots & B_1 & B_0 \\ & & & \ddots & \vdots & \ddots & B_0 \\ & & & & B_W & \cdots & B_1 & B_0 \end{array} \right]}^{nL} \left. \vphantom{\left[ \begin{array}{cccc} B_0 & & B_W & \cdots & B_1 \\ B_1 & B_0 & & & \vdots \\ \vdots & B_1 & B_0 & & B_W \\ B_W & \vdots & B_1 & \ddots & \\ & B_W & \vdots & \ddots & B_0 \\ & & B_W & \ddots & B_1 & B_0 \\ & & & \ddots & \vdots & \ddots & B_0 \\ & & & & B_W & \cdots & B_1 & B_0 \end{array} \right]} \right\}^{mL} \quad (16)$$

The code rate  $R_{\text{SC-PLDPC-TBC}}$  of a SC-PLDPC-TBC is the same as that of its underlying block code, i.e.,

$$R_{\text{SC-PLDPC-TBC}} = \frac{nL - mL}{nL} = R_{\text{PLDPC-BC}}. \quad (17)$$

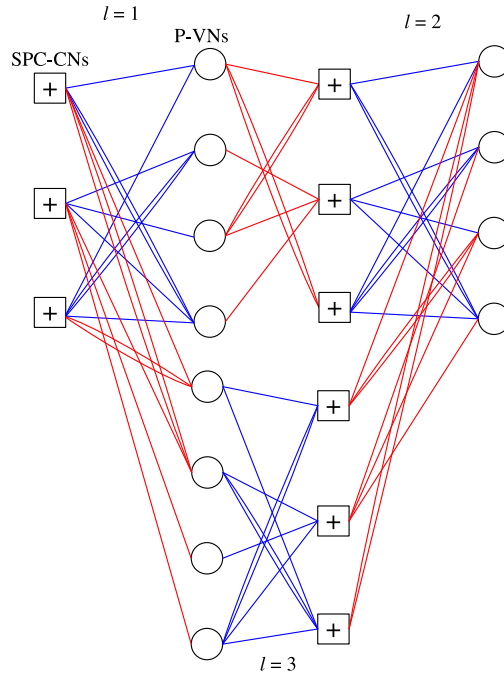


Fig. 6. The protograph of a SC-PLDPC-TBC derived from Fig. 4.  $W = 1$  and  $L = 3$ .

Using the example shown in Fig. 4 and allowing the spatially coupled protographs connected end-to-end, we obtain the spatially coupled tail-biting protograph shown in Fig. 6. The protomatrix of the SC-PLDPC-TBC is given by

$$\mathbf{B}_{\text{TBC}, W=1, L=3} = \begin{bmatrix} \mathbf{B}_0 & \mathbf{B}_1 & \\ \mathbf{B}_1 & \mathbf{B}_0 & \\ & \mathbf{B}_1 & \mathbf{B}_0 \end{bmatrix}. \quad (18)$$

By extending the coupling length  $L$  of a SC-PLDPC-TDC to infinity, a SC-PLDPC-CC is



### III. SPATIALLY COUPLED PLDPC-HADAMARD CONVOLUTIONAL CODES

In this section, we show the details of our proposed spatially coupled PLDPC-Hadamard convolutional codes (SC-PLDPCH-CC). First, we show the way of constructing SC-PLDPCH codes, including SC-PLDPCH tail-biting code (SC-PLDPCH-TBC), SC-PLDPCH terminated code (SC-PLDPCH-TDC) and SC-PLDPCH-CC, from its block code counterpart. Second, we briefly explain the encoding process of SC-PLDPCH-CCs. Third, we describe an efficient decoding algorithm for SC-PLDPCH-CC, which combines the layered decoding used for decoding PLDPCH-BC [21] and the pipeline decoding used for decoding SC-PLDPC-CC [33]. Fourth, we propose a layered PEXIT algorithm for evaluating the theoretical threshold of a SC-PLDPCH-TDC, which is then used to approximate the threshold of the corresponding SC-PLDPCH-CC. Fifth, we propose a genetic algorithm (GA) to optimize the SC-PLDPCH-TDC/SC-PLDPCH-CC designs based on a given PLDPCH-BC.

#### A. Code Construction

Spatially coupled PLDPC-Hadamard codes are constructed in a similar way as SC-PLDPC codes. We also denote the coupling width as  $W$  and coupling length as  $L$  in a SC-PLDPCH code. Given a PLDPC-Hadamard block code with a protomatrix  $\mathbf{B}$ , we apply the edge-spreading procedure to split  $\mathbf{B}$  into  $W + 1$  protomatrices  $\mathbf{B}_i$  ( $i = 0, 1, \dots, W$ ) under the constraint  $\mathbf{B} = \sum_{i=0}^W \mathbf{B}_i$ . Then we couple  $L$  sets of these matrices to construct the protomatrix of a spatially coupled PLDPC-Hadamard code. Similar to the SC-PLDPC codes described in Sect. II-C, a SC-PLDPCH-TDC is formed if the coupled matrices are directly terminated; a SC-PLDPCH-TBC is formed if the coupled matrices are connected end-to-end; and a SC-PLDPCH-CC is formed if the coupling length  $L$  becomes infinite. Since the constructed protomatrices only represent the connections between P-VNs and H-CNs, SC-PLDPC-Hadamard codes have protomatrix structures similar to those of SC-PLDPC codes, i.e., (7) for SC-PLDPCH-TDC; (16) for SC-PLDPCH-TBC; and (19) for SC-PLDPCH-CC. Unlike the protographs of SC-PLDPC codes which consist of P-VNs and SPC-CNs, the protographs of SC-PLDPCH codes contains P-VNs and H-CNs connected with some appropriate D1H-VNs. Fig. 8 shows the protograph of a SC-PLDPCH-CC which is derived from the PLDPCH-BC in Fig. 3.

Using a similar two-step lifting process as that in Sect. II-A, SC-PLDPCH codes can be constructed from the coupled protographs. Assuming that  $\mathbf{B}$  has a constant row weight of  $d$  and



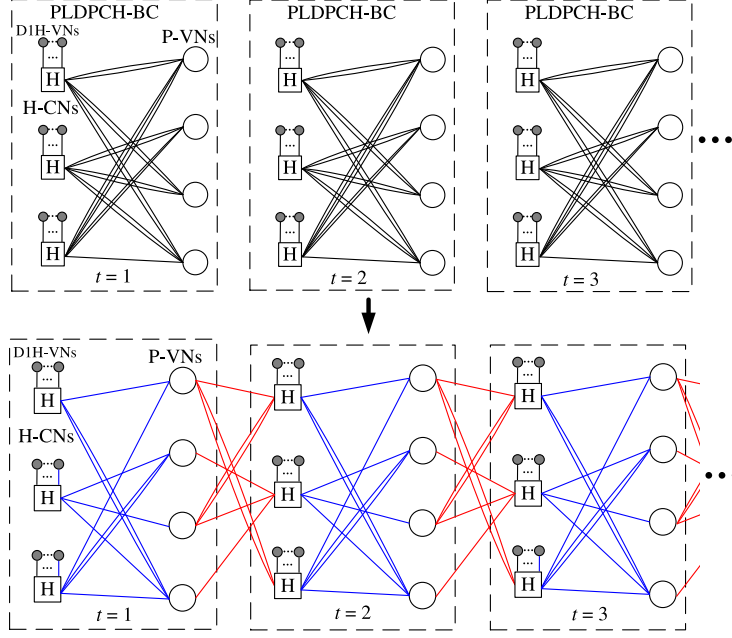


Fig. 8. Protograph of a SC-PLDPCH-CC derived from the PLDPCH-BC in Fig. 3.  $W = 1$ .

hence an order- $r$  ( $= d - 2$ ) Hadamard code is used, it can be readily shown that the code rates of the SC-PLDPCH codes are as follows. For SC-PLDPCH-TDCs, the code rate equals

$$\begin{aligned}
 R_{\text{SC-PLDPCH-TDC}}^{\text{even}} &= \frac{nL - m(L + W)}{nL + m(L + W)(2^r - d)} \\
 &= \frac{n - m\left(1 + \frac{W}{L}\right)}{n + m\left(1 + \frac{W}{L}\right)(2^r - d)} \quad (21)
 \end{aligned}$$

when  $r$  is even, and

$$\begin{aligned}
 R_{\text{SC-PLDPCH-TDC}}^{\text{odd}} &= \frac{nL - m(L + W)}{nL + m(L + W)(2^r - 2)} \\
 &= \frac{n - m\left(1 + \frac{W}{L}\right)}{n + m\left(1 + \frac{W}{L}\right)(2^r - 2)} \quad (22)
 \end{aligned}$$

when  $r$  is odd. For SC-PLDPCH-TBCs and SC-PLDPCH-CCs, their code rates are the same as the block code counterparts, i.e.,

$$\begin{aligned}
 R_{\text{SC-PLDPCH-TBC}}^{\text{even}} &= R_{\text{SC-PLDPCH-CC}}^{\text{even}} \\
 &= R_{\text{PLDPCH-BC}}^{\text{even}} = \frac{n - m}{n + m(2^r - r - 2)} \quad (23)
 \end{aligned}$$

when  $r$  is even, and

$$\begin{aligned} R_{\text{SC-PLDPCH-TBC}}^{\text{odd}} &= R_{\text{SC-PLDPCH-CC}}^{\text{odd}} \\ &= R_{\text{PLDPCH-BC}}^{\text{odd}} = \frac{n - m}{n + m(2^r - 2)} \end{aligned} \quad (24)$$

when  $r$  is odd.

### B. Encoding of SC-PLDPCH-CC

From this point forward and unless otherwise stated, we focus our study on SC-PLDPCH-CC. We also assume that the row weight of  $\mathbf{B}$  equals  $d = r + 2$  and is even. After performing a two-step lifting process on (19), we obtain the semi-infinite parity-check matrix of a SC-PLDPCH-CC in Fig. 9.

Denoting the two lifting factors by  $z_1$  and  $z_2$ , each  $\mathbf{H}_i$  ( $i = 0, 1, \dots, W$ ) has a size of  $M \times N = mz_1z_2 \times nz_1z_2$ . At time  $t$ ,  $M - N$  information bits denoted by  $\mathbf{b}(t) \in \{0, 1\}^{M-N}$  are input to the SC-PLDPCH-CC encoder. The output of the SC-PLDPCH-CC encoder contains  $N$  coded bits corresponding to P-VNs, which are denoted by  $\mathbf{P}(t)$ ; and  $M(2^r - r - 2)$  Hadamard parity-check bits corresponding to D1H-VNs, which are denoted by  $\mathbf{D}(t)$ . Referring to Fig. 9, we generate the output bits as follows.

- 1)  $t = 1$ : Given  $\mathbf{b}(1)$ ,  $\mathbf{P}(1)$  is generated based on the first block row of  $\mathbf{H}_{\text{SC-PLDPCH-CC}}$ , i.e.,  $\mathbf{H}_0$ . Moreover,  $\mathbf{D}(1)$  is computed based on  $[\overbrace{\mathbf{0} \cdots \mathbf{0}}^w \mathbf{P}(1)]$  and the structure  $[\mathbf{H}_W \cdots \mathbf{H}_1 \mathbf{H}_0]$ , where  $\mathbf{0}$  is the length- $N$  zero vector.
- 2)  $t = 2$ : Given  $\mathbf{b}(2)$  and  $\mathbf{P}(1)$ ,  $\mathbf{P}(2)$  is generated based on the second block row of  $\mathbf{H}_{\text{SC-PLDPCH-CC}}$ , i.e.,  $[\mathbf{H}_1 \mathbf{H}_0]$ . Moreover,  $\mathbf{D}(2)$  is computed based on  $[\overbrace{\mathbf{0} \cdots \mathbf{0}}^{w-1} \mathbf{P}(1) \mathbf{P}(2)]$  and the structure  $[\mathbf{H}_W \cdots \mathbf{H}_1 \mathbf{H}_0]$ .
- 3)  $t \leq W$ : Given  $\mathbf{b}(t)$  and  $[\mathbf{P}(1) \mathbf{P}(2) \cdots \mathbf{P}(t-1)]$ ,  $N$  coded bits  $\mathbf{P}(t)$  are generated based on the  $t$ -th block row of  $\mathbf{H}_{\text{SC-PLDPCH-CC}}$ , i.e.,  $[\mathbf{H}_{t-1} \cdots \mathbf{H}_1 \mathbf{H}_0]$ .  $\mathbf{D}(t)$  corresponding to the  $M(2^r - r - 2)$  D1H-VNs are computed based on  $[\overbrace{\mathbf{0} \cdots \mathbf{0}}^{w+1-t} \mathbf{P}(1) \cdots \mathbf{P}(t)]$  and the structure  $[\mathbf{H}_W \mathbf{H}_{W-1} \cdots \mathbf{H}_0]$ .
- 4)  $t > W$ : Given  $\mathbf{b}(t)$  and  $[\mathbf{P}(t-W) \mathbf{P}(t-W+1) \cdots \mathbf{P}(t-1)]$ ,  $\mathbf{P}(t)$  is generated based on the  $t$ -th block row of  $\mathbf{H}_{\text{SC-PLDPCH-CC}}$ , i.e.,  $[\mathbf{H}_W \cdots \mathbf{H}_1 \mathbf{H}_0]$ . Then,  $\mathbf{D}(t)$  is computed based on  $[\mathbf{P}(t-W) \cdots \mathbf{P}(t-1) \mathbf{P}(t)]$  and the structure  $[\mathbf{H}_W \mathbf{H}_{W-1} \cdots \mathbf{H}_0]$ .



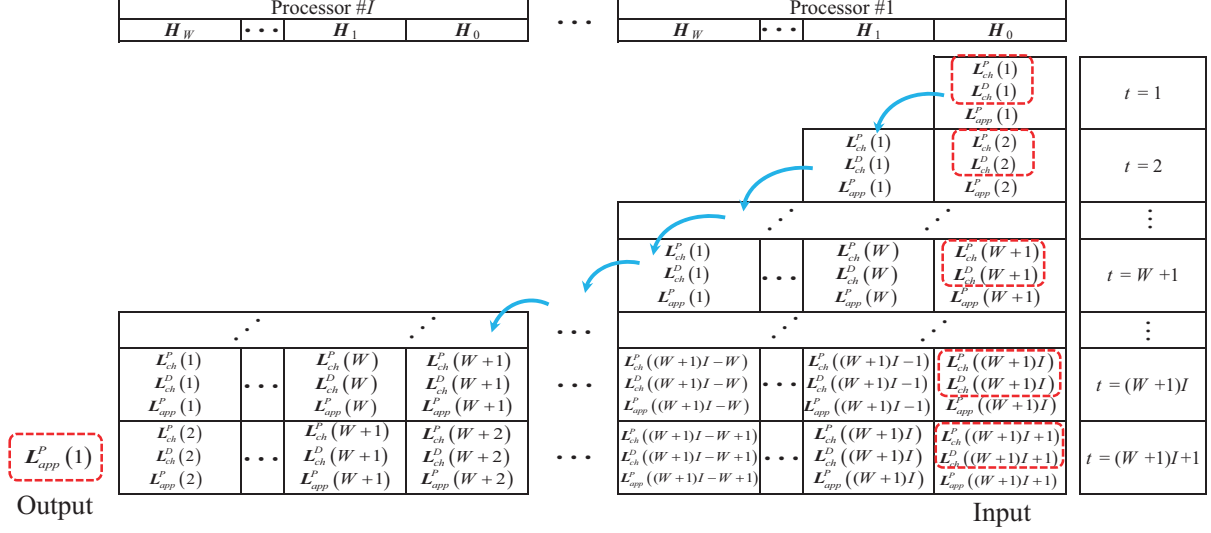


Fig. 10. Structure of a pipeline SC-PLDPCH-CC decoder consisting of  $I$  processors (PLDPC-Hadamard block sub-decoders).  $\{\mathbf{L}_{ch}^P(t), \mathbf{L}_{ch}^D(t)\}$  ( $t = 1, 2, \dots$ ) are input into the decoder one set by one set. Every time, all sets of LLRs inside the decoder are shifted to the left, and all APP-LLRs of all P-VNs inside the different  $I$  processors are updated. When  $\{\mathbf{L}_{ch}^P((W+1)I + t'), \mathbf{L}_{ch}^D((W+1)I + t')\}$  ( $t' = 1, 2, \dots$ ) is input to the decoder, the APP-LLRs  $\mathbf{L}_{app}^P(t')$  are output and the values of the coded bits  $\mathbf{P}(t')$  are determined.

extrinsic LLR information. Here, we apply the layered decoding algorithm [21] in each of these PLDPC-Hadamard block sub-decoders.

We denote the APP-LLR values of the coded bits  $\mathbf{P}(t)$  by  $\mathbf{L}_{app}^P(t)$ . Referring to Fig. 10,  $\{\mathbf{L}_{ch}^P(1), \mathbf{L}_{ch}^D(1)\}$  is first input to the pipeline decoder and Processor #1 updates the APP-LLR of all P-VNs inside, i.e.,  $\mathbf{L}_{app}^P(1)$ . In addition, extrinsic LLR information is updated and stored in the processor but is not depicted in the figure. Then,  $\{\mathbf{L}_{ch}^P(2), \mathbf{L}_{ch}^D(2)\}$  is input to the pipeline decoder while  $\{\mathbf{L}_{ch}^P(1), \mathbf{L}_{ch}^D(1), \mathbf{L}_{app}^P(1)\}$  and related extrinsic LLR information are shifted to the left in the decoder. Processor #1 updates the APP-LLRs of all P-VNs inside, i.e.,  $\mathbf{L}_{app}^P(1)$  and  $\mathbf{L}_{app}^P(2)$ . Again, extrinsic LLR information is updated and stored in the processor but is not depicted. Subsequently,  $\{\mathbf{L}_{ch}^P(t), \mathbf{L}_{ch}^D(t)\}$  ( $t = 3, 4, \dots$ ) are input into the decoder one set by one set. Every time, all sets of LLRs inside the decoder are shifted to the left by one “ $\mathbf{H}_i$ ” block, and all APP-LLRs of all P-VNs inside the different  $I$  processors are updated. Referring to Fig. 10, when  $\{\mathbf{L}_{ch}^P((W+1)I+1), \mathbf{L}_{ch}^D((W+1)I+1)\}$  is input to the pipeline decoder, the APP-LLRs  $\mathbf{L}_{app}^P(1)$  have gone through the iterative process and are output from the decoder. Hard decisions are made based on these APP-LLRs to determine the values of the coded bits  $\mathbf{P}(1)$ . The process continues and every time  $\{\mathbf{L}_{ch}^P((W+1)I+t'), \mathbf{L}_{ch}^D((W+1)I+t')\}$  ( $t' = 1, 2, \dots$ ) is input to the decoder, the APP-LLRs  $\mathbf{L}_{app}^P(t')$  are output and the values of the coded bits  $\mathbf{P}(t')$

are determined.

#### D. Layered PEXIT Algorithm

In [16] and [17], a low-complexity PEXIT chart technique has been proposed to evaluate the theoretical threshold of PLDPCH-BCs. The thresholds of SC-PLDPCH-CCs are expected to be comparable to those of their underlying block codes. However, direct analysis of SC-PLDPCH-CCs with infinite length is very complicated and time-consuming, which is not conducive to the optimal design of the codes in the next section, i.e., Section III-E.

As mentioned in Section III-A, under the same set of split protomatrices  $\{\mathbf{B}_0, \mathbf{B}_1, \dots, \mathbf{B}_W\}$ , SC-PLDPCH-CCs can be obtained by extending the coupling length  $L$  of SC-PLDPCH-TDCs to infinity. A SC-PLDPCH-TDC can be treated as a PLDPCH-BC with a large size and hence its threshold can be evaluated using the original PEXIT chart method in [16] [17]. For SC-PLDPCH-TDCs constructed with different split protomatrices, the original PEXIT chart method will generate different (i.e., distinguishable) thresholds<sup>2</sup>. For example, Fig. 11 shows the thresholds for two different SC-PLDPCH-TDCs using the original PEXIT chart method. We set  $W = 1$ . Based on the optimal protomatrix  $\mathbf{B}$  in [16] [17], i.e.,

$$\mathbf{B} = \begin{bmatrix} 1 & 0 & 0 & 0 & 0 & 0 & 1 & 0 & 3 & 0 & 1 \\ 0 & 1 & 2 & 0 & 0 & 0 & 0 & 0 & 0 & 2 & 1 \\ 2 & 1 & 0 & 0 & 1 & 1 & 0 & 0 & 0 & 0 & 1 \\ 0 & 1 & 0 & 3 & 0 & 0 & 0 & 0 & 0 & 2 & 0 \\ 2 & 0 & 0 & 0 & 0 & 0 & 0 & 1 & 0 & 3 & 0 \\ 3 & 0 & 0 & 2 & 0 & 0 & 1 & 0 & 0 & 0 & 0 \\ 1 & 0 & 0 & 1 & 1 & 0 & 0 & 0 & 1 & 2 & 0 \end{bmatrix}, \quad (25)$$

the split protomatrices of SC-PLDPCH-TDC #1 are

$$\mathbf{B}_0 = \begin{bmatrix} 1 & 0 & 0 & 0 & 0 & 0 & 0 & 0 & 0 & 0 & 1 \\ 0 & 0 & 1 & 0 & 0 & 0 & 0 & 0 & 0 & 1 & 0 \\ 1 & 0 & 0 & 0 & 0 & 0 & 0 & 0 & 0 & 0 & 0 \\ 0 & 0 & 0 & 3 & 0 & 0 & 0 & 0 & 0 & 2 & 0 \\ 0 & 0 & 0 & 0 & 0 & 0 & 0 & 0 & 0 & 0 & 0 \\ 1 & 0 & 0 & 2 & 0 & 0 & 1 & 0 & 0 & 0 & 0 \\ 0 & 0 & 0 & 0 & 0 & 0 & 0 & 0 & 1 & 0 & 0 \end{bmatrix} \quad (26)$$

<sup>2</sup>For SC-PLDPCH-TDCs constructed with different split protomatrices but arrived at the same threshold, we further verify their error performance by simulations.

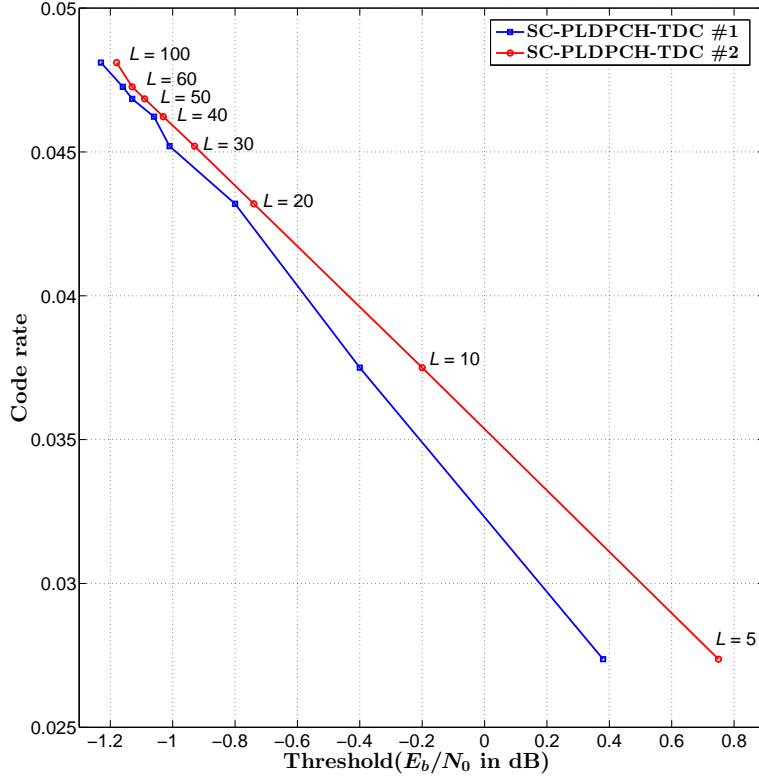


Fig. 11. Distinguishable thresholds for two different SC-PLDPCH-TDCs corresponding to different set of protomatrices  $\{\mathbf{B}_0, \mathbf{B}_1\}$ . Their underlying block code is the optimal  $r = 4$  PLDPCH-BC [16] [17].  $W = 1$ .

and

$$\mathbf{B}_1 = \begin{bmatrix} 0 & 0 & 0 & 0 & 0 & 0 & 1 & 0 & 3 & 0 & 0 \\ 0 & 1 & 1 & 0 & 0 & 0 & 0 & 0 & 0 & 1 & 1 \\ 1 & 1 & 0 & 0 & 1 & 1 & 0 & 0 & 0 & 0 & 1 \\ 0 & 1 & 0 & 0 & 0 & 0 & 0 & 0 & 0 & 0 & 0 \\ 2 & 0 & 0 & 0 & 0 & 0 & 0 & 1 & 0 & 3 & 0 \\ 2 & 0 & 0 & 0 & 0 & 0 & 0 & 0 & 0 & 0 & 0 \\ 1 & 0 & 0 & 1 & 1 & 0 & 0 & 0 & 0 & 2 & 0 \end{bmatrix}; \quad (27)$$

and the split protomatrices of SC-PLDPCH-TDC #2 are

$$\mathbf{B}_0 = \begin{bmatrix} 0 & 0 & 0 & 0 & 0 & 0 & 0 & 0 & 0 & 0 & 0 \\ 0 & 1 & 2 & 0 & 0 & 0 & 0 & 0 & 0 & 0 & 0 \\ 2 & 1 & 0 & 0 & 1 & 0 & 0 & 0 & 0 & 0 & 1 \\ 0 & 0 & 0 & 3 & 0 & 0 & 0 & 0 & 0 & 1 & 0 \\ 0 & 0 & 0 & 0 & 0 & 0 & 0 & 1 & 0 & 3 & 0 \\ 2 & 0 & 0 & 1 & 0 & 0 & 0 & 0 & 0 & 0 & 0 \\ 1 & 0 & 0 & 1 & 0 & 0 & 0 & 0 & 0 & 0 & 0 \end{bmatrix} \quad (28)$$

and

$$\mathbf{B}_1 = \begin{bmatrix} 1 & 0 & 0 & 0 & 0 & 0 & 1 & 0 & 3 & 0 & 1 \\ 0 & 0 & 0 & 0 & 0 & 0 & 0 & 0 & 0 & 2 & 1 \\ 0 & 0 & 0 & 0 & 0 & 1 & 0 & 0 & 0 & 0 & 0 \\ 0 & 1 & 0 & 0 & 0 & 0 & 0 & 0 & 0 & 1 & 0 \\ 2 & 0 & 0 & 0 & 0 & 0 & 0 & 0 & 0 & 0 & 0 \\ 1 & 0 & 0 & 1 & 0 & 0 & 1 & 0 & 0 & 0 & 0 \\ 0 & 0 & 0 & 0 & 1 & 0 & 0 & 0 & 1 & 2 & 0 \end{bmatrix}, \quad (29)$$

where  $\mathbf{B}_0 + \mathbf{B}_1 = \mathbf{B}$ . From Fig. 11, we can observe that the thresholds of two SC-PLDPCH-TDCs are distinguishable and reduced as  $L$  increases. Subsequently, we select the protomatrices with good thresholds (i.e., low  $E_b/N_0$ ) to construct the corresponding convolutional codes (i.e., SC-PLDPCH-CCs).

To improve the convergence rate of the original PEXIT chart method, we propose a layered PEXIT method to analyze the SC-PLDPCH-TDCs. We first define the following symbols.

- $I_{av}(i, j)$ : the *a priori* mutual information (MI) from the  $i$ -th H-CN to the  $j$ -th P-VN
- $I_{ev}(i, j)$ : the extrinsic MI from the  $j$ -th P-VN to the  $i$ -th H-CN
- $I_{ah}(k)$ : the *a priori* MI of the  $k$ -th information bit in the  $i$ -th H-CN
- $I_{eh}(k)$ : the extrinsic MI of the  $k$ -th information bit in the  $i$ -th H-CN
- $I_{app}(j)$ : the *a posteriori* MI of the  $j$ -th P-VN
- $\sigma_{app}(j)$ : the *a posteriori* information of the  $j$ -th P-VN
- $\sigma_{temp}(j)$ : the temporary value of  $\sigma_{app}(j)$

We also assume that the channel LLR value  $L_{ch}$  follows a normal distribution  $\mathcal{N}(\sigma_{L_{ch}}^2/2, \sigma_{L_{ch}}^2)$ , where  $\sigma_{L_{ch}}^2 = 8R \cdot E_b/N_0$ ,  $R$  is the code rate of SC-PLDPCH-TDC, and  $E_b/N_0$  is the bit-energy-to-noise-power-spectral-density ratio. When the output MI from P-VN or H-CN processors is  $I_{MI}$ , we suppose that the corresponding LLR values of the extrinsic information obey a normal distribution  $\mathcal{N}(\pm\sigma^2/2, \sigma^2)$ . The relationship between  $I_{MI}$  and  $\sigma$  can be approximately computed by the functions  $I_{MI} = J(\sigma)$  and  $\sigma = J^{-1}(I_{MI})$  in [35], [36].

Given a coupling width  $W$  and a set of protomatrices  $\{\mathbf{B}_0, \mathbf{B}_1, \dots, \mathbf{B}_W\}$  each of size  $m \times n$ , we use these protomatrices to construct a SC-PLDPCH-TDC with the coupling width  $W$  and an appropriate coupling length  $L$ . The protomatrix of the SC-PLDPCH-TDC  $\mathbf{B}_{\text{SC-PLDPCH-TDC}} = \{b_{\text{TDC}}(i, j)\}$  therefore has a size of  $m(L + W) \times nL$ . In (30), the protomatrix  $\mathbf{B}$  of size  $m \times n = 3 \times 4$  is split into  $\mathbf{B}_0$  and  $\mathbf{B}_1$  of the same size assuming  $W = 1$ . Based on  $\mathbf{B}_0$  and  $\mathbf{B}_1$ , a SC-PLDPCH-TDC with  $W = 1$  and  $L = 2$  is constructed in (31) and has a size of

$$\mathbf{B} = \begin{bmatrix} 2 & 0 & 2 & 2 \\ 0 & 2 & 2 & 2 \\ 3 & 2 & 0 & 1 \end{bmatrix}, \mathbf{B}_0 = \begin{bmatrix} 1 & 0 & 0 & 2 \\ 0 & 1 & 1 & 1 \\ 1 & 2 & 0 & 1 \end{bmatrix}, \mathbf{B}_1 = \begin{bmatrix} 1 & 0 & 2 & 0 \\ 0 & 1 & 1 & 1 \\ 2 & 0 & 0 & 0 \end{bmatrix} \quad (30)$$

$$\mathbf{B}_{\text{SC-PLDPCH-TDC}} = \begin{bmatrix} \mathbf{B}_0 & \mathbf{0} \\ \mathbf{B}_1 & \mathbf{B}_0 \\ \mathbf{0} & \mathbf{B}_1 \end{bmatrix} = \begin{bmatrix} 1 & 0 & 0 & 2 & 0 & 0 & 0 & 0 \\ 0 & 1 & 1 & 1 & 0 & 0 & 0 & 0 \\ 1 & 2 & 0 & 1 & 0 & 0 & 0 & 0 \\ 1 & 0 & 2 & 0 & 1 & 0 & 0 & 2 \\ 0 & 1 & 1 & 1 & 0 & 1 & 1 & 1 \\ 2 & 0 & 0 & 0 & 1 & 2 & 0 & 1 \\ 0 & 0 & 0 & 0 & 1 & 0 & 2 & 0 \\ 0 & 0 & 0 & 0 & 0 & 1 & 1 & 1 \\ 0 & 0 & 0 & 0 & 2 & 0 & 0 & 0 \end{bmatrix} \quad (31)$$

$$\sigma_{temp}(j) = \sqrt{(\sigma_{app}(j))^2 - b_{\text{TDC}}(i, j) \times (J^{-1}(I_{av}(i, j)))^2} \forall j \quad (32)$$

$$I_{ev}(i, j) = J \left( \sqrt{(\sigma_{app}(j))^2 - (J^{-1}(I_{av}(i, j)))^2} \right) \forall j \quad (33)$$

$$\mathbf{b}_{\text{TDC}}(1, :) = [1 \ 0 \ 0 \ 2 \ 0 \ 0 \ 0 \ 0] \quad (34)$$

$$\mathbf{I}_{ev}(1, :) = [I_{ev}(1, 1) \ 0 \ 0 \ I_{ev}(1, 4) \ 0 \ 0 \ 0 \ 0] \quad (35)$$

$$\begin{aligned} \mathbf{I}_{ah} &= [I_{ah}(1) \ I_{ah}(2) \ I_{ah}(3) \ I_{ah}(4) \ I_{ah}(5) \ I_{ah}(6)] \\ &= [1 \ 1 \ 1 \ I_{ev}(1, 1) \ I_{ev}(1, 4) \ I_{ev}(1, 4)] \end{aligned} \quad (36)$$

$$I_{eh}(k) = \frac{1}{2} \sum_{x \in \{0,1\}} \int_{-\infty}^{\infty} p_e(\xi|X=x) \log_2 \frac{2 \cdot p_e(\xi|X=x)}{p_e(\xi|X="0") + p_e(\xi|X="1")} d\xi \quad (37)$$

$$\approx 1 - \frac{1}{w} \sum_{\alpha=1}^w \log_2 \left( 1 + e^{-(1-2U(\alpha, k)) \times V(\alpha, k)} \right) \quad (38)$$

$$\mathbf{I}_{eh} = [I_{eh}(1) \ I_{eh}(2) \ I_{eh}(3) \ I_{eh}(4) \ I_{eh}(5) \ I_{eh}(6)] \quad (39)$$

$$\mathbf{I}_{av}(1, :) = [I_{av}(1, 1) \ 0 \ I_{av}(1, 3) \ 0 \ 0 \ 0 \ 0 \ 0] \quad (40)$$

$$= \left[ I_{eh}(4) \ 0 \ \frac{1}{2} \sum_{k=5}^6 I_{eh}(k) \ 0 \ 0 \ 0 \ 0 \ 0 \right] \quad (41)$$

$$\sigma_{app}(j) = \sqrt{(\sigma_{temp}(j))^2 + b_{\text{TDC}}(i, j) \times (J^{-1}(I_{av}(i, j)))^2} \forall j \quad (42)$$

$m(L + W) \times nL = 9 \times 8$ . Note that in computing the threshold of the SC-PLDPCH-TDC, a larger  $L$ , e.g.,  $L = 10$ , will be used for threshold evaluation such that  $nL > m(L + W)$ .

Similar to the decoding strategy in the layered decoder [21], the layered PEXIT method proceeds as follows.

- 1) Set the initial  $E_b/N_0$  in dB (i.e.,  $E_b/N_0(\text{dB})$ )<sup>3</sup>.
- 2) Set the maximum number of iterations  $N_{\text{max}} = 150$ .

<sup>3</sup>The initial values will be different according to different codes (corresponding to different Hadamard order  $r$ ). In our optimization design, given  $W = 1$  and  $L = 10$ , initial  $E_b/N_0$  is  $-0.30$  dB for  $r = 4$ ,  $-0.40$  dB for  $r = 5$ ,  $-0.80$  dB for  $r = 8$  and  $-0.85$  dB for  $r = 10$ , respectively.



- 3) Compute  $\sigma_{L_{ch}} = (8R \cdot 10^{(E_b/N_0(\text{dB}))/10})^{1/2}$  for  $L_{ch}$ , and set  $\sigma_{app}(j) = \sigma_{L_{ch}}$  for  $j = 1, 2, \dots, nL$ .
- 4) For  $i = 1, 2, \dots, m(L + W)$  and  $j = 1, 2, \dots, nL$ , set  $I_{av}(i, j) = 0$ .
- 5) Set the iteration number  $N_{it} = 1$ .

6) Set  $i = 1$ .

- 7) For  $j = 1, 2, \dots, nL$ , subtract  $b_{\text{TDC}}(i, j) \times (J^{-1}(I_{av}(i, j)))^2$  from  $(\sigma_{app}(j))^2$ , and then compute  $\sigma_{temp}(j)$  using (32).

- 8) For  $j = 1, 2, \dots, nL$ , compute (33) if  $b_{\text{TDC}}(i, j) > 0$ ; otherwise set  $I_{ev}(i, j) = 0$ .

Taking the first row of the  $9 \times 8$  protomatrix  $\mathbf{B}_{\text{SC-PLDPCH-TDC}}$  in (31) as an example, we obtain the  $1 \times 8$  vector  $\mathbf{b}_{\text{TDC}}(1, :)$  shown in (34). After analyzing the MI of the P-VNs, the corresponding  $1 \times 8$  MI vector  $\mathbf{I}_{ev}(1, :)$  is shown in (35).

- 9) Convert the  $1 \times nL$   $\mathbf{I}_{ev}(i, :)$  MI vector into a  $1 \times d$   $\mathbf{I}_{ah}$  MI vector by eliminating the 0 entries and repeating  $b_{\text{TDC}}(i, j) (\geq 1)$  times the entry  $I_{ev}(i, j)$ .

*Remark:* Each row weight of a protomatrix  $\mathbf{B}$  for the underlying PLDPCH-BC equals  $d = r + 2$  [16] [17] and hence each row corresponds to a  $r = d - 2$  Hadamard code. However, due to the structure of SC-PLDPCH-TDCs, the first and last  $Wm$  rows in  $\mathbf{B}_{\text{SC-PLDPCH-TDC}}$  contain only part of the structure  $[\mathbf{B}_W \dots \mathbf{B}_1 \mathbf{B}_0]$  ( $\mathbf{B} = \sum_{i=0}^W \mathbf{B}_i$ ) and thus the row weight could be less than  $d$ . For simplicity and uniformity, we compute the MI values of  $r = d - 2$  Hadamard code for each row (i.e., each H-CN). For the first/last  $Wm$  rows in  $\mathbf{B}_{\text{SC-PLDPCH-TDC}}$ , when their row weight  $d_1$  is less than  $d$ , the first/last  $d - d_1$  MI values in  $\mathbf{I}_{ah}$  are set to 1<sup>4</sup>. For example, the row weight of the underlying protomatrix  $\mathbf{B}$  (30) equals  $d = 6$  while the row weight of the  $1 \times 8$   $\mathbf{b}_{\text{TDC}}(1, :)$  equals  $d_1 = 3 < d$ . Hence, when converting  $1 \times 8$   $\mathbf{I}_{ev}(1, :)$  into the  $1 \times 6$   $\mathbf{I}_{ah}$  MI vector, the first  $d - d_1 = 3$  values, i.e.,  $[I_{ah}(1) I_{ah}(2) I_{ah}(3)]$  are set to 1, as shown in (36).

- 10) Based on  $\sigma_{L_{ch}}$  and the  $d$  entries in  $\mathbf{I}_{ah}$ , we use the Monte Carlo method in [16], [17] to generate  $d$  extrinsic MI values, i.e., a  $1 \times d$  MI vector  $\mathbf{I}_{eh}$ <sup>5</sup>. (For more details of the method, please refer to the Appendices in [16], [17].) We use the same symbol definitions as in [16], [17]. Hence  $p_e(\xi|X = x)$  in (37) denotes the PDF of the LLR values given the bit  $x$  being “0” or “1”; in (38),  $\mathbf{U} = \{U(\alpha, k)\}$  denotes a  $w \times d$  matrix in which each row represents a length- $d$  SPC codeword and  $\mathbf{V} = \{V(\alpha, k)\}$  denotes a  $w \times d$  matrix in which each row

<sup>4</sup>MI value equal to 1 means that the corresponding MI is known and does not provide any new information in the analysis.

<sup>5</sup>When MI value equals 1, Monte Carlo method will generate the corresponding LLR values with large absolute values. In our analysis, we set them as  $\pm 100$ .

represents a set of ( $d$ ) extrinsic LLR values generated by the Hadamard decoder.

Using the previous example, the MI vector  $\mathbf{I}_{eh}$  is shown in (39).

- 11) Convert the  $1 \times d$   $\mathbf{I}_{eh}$  MI vector into a  $1 \times nL$   $\mathbf{I}_{av}(i, :)$  MI vector. For  $j = 1, 2, \dots, nL$ , if  $b_{\text{TDC}}(i, j) > 0$ , set the value of  $I_{av}(i, j)$  as the average of the corresponding  $b_{\text{TDC}}(i, j)$  MI values in  $\mathbf{I}_{eh}$ ; otherwise set  $I_{av}(i, j) = 0$ . For the first/last  $Wm$  rows in  $\mathbf{B}_{\text{SC-PLDPCH-TDC}}$ , when their row weight  $d_1$  is less than  $d$ , the first/last  $d - d_1$  MI values in  $\mathbf{I}_{eh}$  will be omitted, and the remaining  $d_1$  values will be used to compute  $\mathbf{I}_{av}(i, :)$ .

In the above example, we omit the first  $d - d_1 = 3$  MI values in  $\mathbf{I}_{eh}$ , i.e.,  $[I_{eh}(1) I_{eh}(2) I_{eh}(3)]$ , and use the remaining  $d_1 = 3$  MI values, i.e.,  $[I_{eh}(4) I_{eh}(5) I_{eh}(6)]$  to compute the  $\mathbf{I}_{av}(1, :)$  MI vector given in (41).

- 12) For  $j = 1, 2, \dots, nL$ , use the “new” extrinsic information  $\mathbf{I}_{av}(i, :)$  to update the *a posteriori* information  $\sigma_{app}(j)$  by (42).
- 13) If  $i$  is smaller than the number of rows, i.e.,  $i < m(L + W)$ , increment  $i$  by 1 and go to Step 7).
- 14) For  $j = 1, 2, \dots, nL$ , compute  $I_{app}(j) = J(\sigma_{app}(j))$ . If  $I_{app}(j) = 1 \forall j$ , decrement  $E_b/N_0$  by 0.05 dB and go to Step 3);
- 15) If the maximum number of iterations is not reached, increment the iteration number  $N_{it}$  by 1 and go to Step 6); otherwise, stop and the threshold is given by  $(E_b/N_0)^* = E_b/N_0 + 0.05$  dB.

As can be observed, the proposed layered PEXIT chart algorithm updates the corresponding *a posteriori* information (using Step 12)) everytime the extrinsic MI of one row (layer) is obtained. Further, we set  $L = 10$  and construct a SC-PLDPCH-TDC with a protomatrix  $\mathbf{B}_{\text{SC-PLDPCH-TDC}}$  of size  $77 \times 110$  (where  $\mathbf{B}_0$  is given by (26) and  $\mathbf{B}_1$  is given by (27)). Table I lists the number of iterations required for the original PEXIT algorithm [16], [17] and our proposed layered PEXIT algorithm to converge as  $E_b/N_0$  changes from  $-0.30$  dB to  $-0.40$  dB. We observe that our layered PEXIT algorithm reduces the number of iterations by at least 30% compared with the original PEXIT algorithm. The number of iterations is reduced by 62.8% at  $E_b/N_0 = -0.40$  dB. We also find that both algorithms do not converge at  $E_b/N_0 = -0.45$  dB when the maximum number of iterations is set to  $N_{\text{max}} = 150$  for the layered PEXIT chart method, and is set to  $2N_{\text{max}} = 300$  for original PEXIT chart method. Thus both algorithms arrive at the same decoding threshold, i.e.,  $(E_b/N_0)^* = -0.40$  dB. The proposed layered PEXIT algorithm can

TABLE I  
 NUMBER OF ITERATIONS  $N_{it}$  REQUIRED FOR THE PEXIT ALGORITHMS TO CONVERGE AT DIFFERENT  $E_b/N_0$ . THE  
 MAXIMUM NUMBER OF ITERATIONS IS  $N_{max} = 150$  FOR THE LAYERED PEXIT CHART ALGORITHM AND  $2N_{max} = 300$  FOR  
 THE ORIGINAL PEXIT CHART ALGORITHM.

$E_b/N_0$ in dB	-0.30	-0.35	-0.40
Original PEXIT [16], [17]	107	190	197
Proposed layered PEXIT	80	104	121

therefore speed up the convergence rate when calculating the threshold of SC-PLDPCH-TDCs.

*Remark:* The difference between our proposed layered PEXIT algorithm and the shuffled EXIT algorithm [37] are as follows.

- Given a protomatrix, our algorithm performs the analysis row by row, while the shuffled EXIT algorithm [37] performs the analysis column by column.
- When analyzing SC-PLDPCH-TDCs, our algorithm computes MI values for Hadamard check nodes, while [37] computes MI values for SPC-CNs.

#### E. Optimizing Protomatrices using Genetic Algorithm

By simulating the evolutionary mechanism of “survival of the fittest” in nature, Holland first proposed using genetic algorithm (GA) in the 1970s [38] to solve optimization problems. A GA involves the following entities.

- *Generation group:* a collection of samples of the search space and also candidate solutions to the problem.
- *Fitness function:* an objective function of the problem which guides the group to optimize in the most favorable direction.
- *Selection process:* duplicating individuals in the parent generation group and forming the offspring generation group.
- *Crossover process:* exchanging parts between individuals in the same generation group.
- *Mutation process:* enriching and expanding the search space by modifying one or more parts of an individual so as to prevent the final solution from falling into local optimals.

To solve a problem based on GA, a generation group is first created or initialized and a fitness function is developed to calculate the fitness value of each individual in the group. Based on the fitness values, some individuals are selected from the “parent” generation group to form an

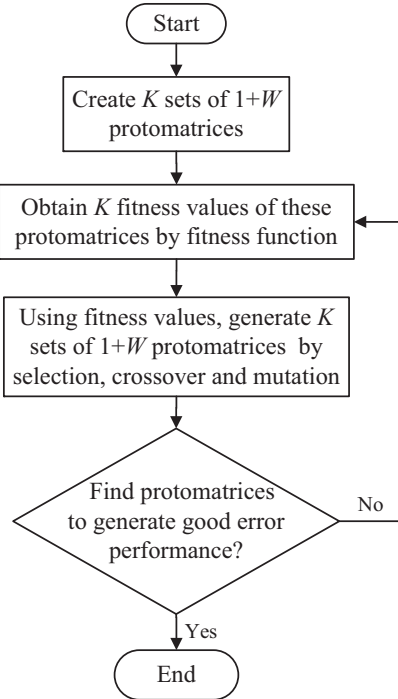


Fig. 12. Flowchart of using GA to search for protomatrices of SC-PLDPC-CCs.

“offspring” generation group. To facilitate obtaining the optimal solution, the individuals having the best fitness values in the parent generation group will be kept in the offspring generation group. Crossover and mutation operations are further performed in the offspring generation group. Subsequently, the “offspring” generation group becomes the “parent” generation group. By repeating the generation cycles, GA has a high probability of arriving at the global optimal solution to the problem [27].

Given a protomatrix  $\mathbf{B}$  corresponding to a PLDPCH-BC, we propose a GA to systematically search for optimized sets of protomatrices  $\{\mathbf{B}_0, \mathbf{B}_1, \dots, \mathbf{B}_W\}$  (where  $\mathbf{B} = \sum_{i=0}^W \mathbf{B}_i$ ) for the corresponding SC-PLDPCH-TDC. By selecting SC-PLDPCH-TDCs with good thresholds, our final objective is to design optimal SC-PLDPCH-CCs based on the same set of protomatrices. We denote

- $K$  parent individuals  $\Phi^k$  ( $k = 1, 2, \dots, K$ ) as  $K$  sets of  $W + 1$  protomatrices, i.e.,  $\Phi^k = \{\mathbf{B}_0^k, \mathbf{B}_1^k, \dots, \mathbf{B}_W^k\}$ , each of which satisfies  $\mathbf{B} = \sum_{i=0}^W \mathbf{B}_i^k$ ;
- the fitness function as  $\psi(\cdot)$  and the fitness value of the  $k$ -th parent individual as  $f_k = \psi(\Phi^k)$ ;
- the probability of selecting the  $k$ -th parent individual as  $p_{s_k}$ ;
- the probability of crossover as  $p_c$ ;

- the probability of mutation as  $p_m$ ;
- $K$  offspring individuals  $\Upsilon_k$  ( $k = 1, 2, \dots, K$ ) as  $K$  sets of  $W + 1$  protomatrices, i.e.,  $\Upsilon_k = \{\mathbf{S}_0^k, \mathbf{S}_1^k, \dots, \mathbf{S}_W^k\}$ , each of which satisfies  $\mathbf{B} = \sum_{i=0}^W \mathbf{S}_i^k$ ;
- $m \times n$  as the size of  $\mathbf{B}$ , and hence also the size of  $\mathbf{B}_i^k$  and  $\mathbf{S}_i^k$  for all  $i$  and  $k$ ;
- $N_g$  as the number of individuals having good fitness values.

Fig. 12 shows the flowchart of our proposed GA and the details of the algorithm are described as follows.

- 1) Initialization: Set coupling width  $W$ , coupling length  $L$ , and the number of individuals  $K$  in each generation. Randomly generate  $K$  sets of  $\Phi^k = \{\mathbf{B}_0^k, \mathbf{B}_1^k, \dots, \mathbf{B}_W^k\}$ ,  $k = 1, 2, \dots, K$ .
- 2) Computation of fitness values: For each  $\Phi^k$ , we construct the corresponding SC-PLDPCH-TDC by coupling  $L$  sets of  $\Phi^k$ . Then we apply our proposed layered PEXIT chart method in Sect. III-D to analyze the threshold and convergence behavior of the SC-PLDPCH-TDC. Recall that for a specific  $E_b/N_0$  value (in dB), the iteration number required to converge is given by  $N_{it}$  and the maximum number of iterations is given by  $N_{max}$ . Our proposed fitness function  $\psi(\cdot)$  takes both the number of successful convergences, denoted by  $N_c$ , and the convergence rate  $N_{it}$  into consideration. We define  $\psi(\cdot)$  as

$$f_k = \psi(\Phi^k) = \sum_{i=1}^{N_c} [N_{max} - N_{it,i}^k] = N_c N_{max} - \sum_{i=1}^{N_c} N_{it,i}^k \quad (43)$$

where  $N_{it,i}^k$  represents the number of iterations for the SC-PLDPCH-TDC corresponding to  $\Phi^k$  to converge in the  $i$ -th successful convergence ( $i = 1, 2, \dots, N_c$ ). Note that  $\psi(\Phi^k)$  should give a larger value if the corresponding SC-PLDPCH-TDC converges faster and more times in the layered PEXIT algorithm.

In the example given in Table I, the layered PEXIT algorithm has converged at  $-0.30$  dB,  $-0.35$  dB and  $-0.40$  dB, and hence  $N_c = 3$ . Using (43), the fitness value of  $\{\mathbf{B}_0, \mathbf{B}_1\}$  defined in (26) and (27) is therefore given by

$$\psi(\{\mathbf{B}_0, \mathbf{B}_1\}) = 3 \times 150 - (80 + 104 + 121) = 145. \quad (44)$$

- 3) Selection: Compute the fitness values  $f_k = \psi(\Phi^k)$  for the  $K$  parent individuals  $\Phi^k$  ( $k = 1, 2, \dots, K$ ). Subsequently, we normalize  $f_k$  ( $k = 1, 2, \dots, K$ ) to form the probabilities of

selection, i.e.,

$$p_{s_k} = f_k / \sum_{j=1}^K f_j; \quad k = 1, 2, \dots, K. \quad (45)$$

Then the  $K$  offspring individuals  $\Upsilon_{k'}$  ( $k' = 1, 2, \dots, K$ ) are chosen from the parent generation group  $\Phi^k$  ( $k = 1, 2, \dots, K$ ) as follows. First, the  $N_g$  individuals with the highest fitness values in the parent group are passed to the offspring group directly to fill  $\Upsilon_{k'}$  ( $k' = 1, 2, \dots, N_g$ ). Then to fill each of the remaining  $K - N_g$  offspring slots, i.e.,  $\Upsilon_{k'}$  ( $k' = N_g + 1, N_g + 2, \dots, K$ ), a random parent individual  $\Phi^k$  is selected accordingly to the probability  $p_{s_k}$ . These  $K - N_g$  offsprings will further go through the crossover and mutation processes below.

- 4) Crossover: Assuming  $K - N_g$  is even, the  $K - N_g$  selected offspring individuals, i.e.,  $\Upsilon_{k'}$  ( $k' = N_g + 1, N_g + 2, \dots, K$ ) are randomly divided into  $(K - N_g)/2$  pairs. For each pair  $\Upsilon_{k_1} = \{\mathbf{S}_0^{k_1}, \mathbf{S}_1^{k_1}, \dots, \mathbf{S}_W^{k_1}\}$  and  $\Upsilon_{k_2} = \{\mathbf{S}_0^{k_2}, \mathbf{S}_1^{k_2}, \dots, \mathbf{S}_W^{k_2}\}$ , we select two random positions  $(u_1, v_1)$  and  $(u_2, v_2)$  where  $1 \leq u_1 \leq u_2 \leq m$  and  $1 \leq v_1 \leq v_2 \leq n$ . With a probability of  $p_c$ , all entries between  $(u_1, v_1)$  and  $(u_2, v_2)$  (in a column-wise manner) in  $\mathbf{S}_i^{k_1}$  are exchanged with the corresponding entries in  $\mathbf{S}_i^{k_2}$  ( $i = 0, 1, \dots, W$ ).

Fig. 13 shows a crossover example where  $m \times n = 3 \times 4$ . The pair of offspring individuals selected are given by  $\Upsilon_{k_1} = \{\mathbf{S}_0^{k_1}, \mathbf{S}_1^{k_1}\}$  and  $\Upsilon_{k_2} = \{\mathbf{S}_0^{k_2}, \mathbf{S}_1^{k_2}\}$  ( $N_g < k_1 \neq k_2 \leq K$ ). The two selected positions are  $(u_1, v_1) = (2, 2)$  and  $(u_2, v_2) = (2, 3)$ . Hence the entries in positions  $(2, 2), (3, 2), (1, 3), (2, 3)$  are exchanged between  $\mathbf{S}_0^{k_1}$  and  $\mathbf{S}_0^{k_2}$ ; and are exchanged between  $\mathbf{S}_1^{k_1}$  and  $\mathbf{S}_1^{k_2}$ .

- 5) Mutation: The offspring individuals  $\Upsilon_{k'} = \{\mathbf{S}_0^{k'}, \mathbf{S}_1^{k'}, \dots, \mathbf{S}_W^{k'}\}$  that have gone through the crossover process will then be considered for mutation separately. Within each offspring individual, one random position  $(u, v)$  ( $1 \leq u \leq m$  and  $1 \leq v \leq n$ ) corresponding to a non-zero entry in  $\mathbf{B}$  are selected. For all the  $(u, v)$ -th entries in  $\mathbf{S}_0^{k'}, \mathbf{S}_1^{k'}, \dots, \mathbf{S}_W^{k'}$ , they are mutated together with a probability of  $p_m$ . The entries should have different values after the mutation while keeping  $\sum_{i=0}^W \mathbf{S}_i^{k'} = \mathbf{B}$  satisfied.

Fig. 14 illustrates a mutation example. The offspring individual being considered is  $\Upsilon_{k_1} = \{\mathbf{S}_0^{k_1}, \mathbf{S}_1^{k_1}\}$  ( $N_g < k_1 \leq K$ ) and mutation occurs in all the  $(3, 1)$ -th entries, where the  $(3, 1)$ -th entry in  $\mathbf{B} = \mathbf{S}_0^{k_1} + \mathbf{S}_1^{k_1}$  (30) equals 3 and hence is non-zero.

- 6) Set  $\Phi_k = \Upsilon_k$ ,  $k = 1, 2, \dots, K$ .  
 7) Repeat Steps 2) to 6) until  $\exists \Phi_k$  such that the corresponding SC-PLDPCH-TDC has a low

$$\begin{array}{cc}
\mathbf{S}_0^{k_1} = \begin{bmatrix} 1 & 0 & 1 & 0 \\ 0 & 2 & 0 & 1 \\ 1 & 1 & 0 & 0 \end{bmatrix} & \mathbf{S}_1^{k_1} = \begin{bmatrix} 1 & 0 & 1 & 2 \\ 0 & 0 & 2 & 1 \\ 2 & 1 & 0 & 1 \end{bmatrix} \\
\mathbf{S}_0^{k_2} = \begin{bmatrix} 1 & 0 & 1 & 1 \\ 0 & 1 & 1 & 1 \\ 0 & 1 & 0 & 1 \end{bmatrix} & \mathbf{S}_1^{k_2} = \begin{bmatrix} 1 & 0 & 1 & 1 \\ 0 & 1 & 1 & 1 \\ 3 & 1 & 0 & 0 \end{bmatrix} \\
\downarrow \text{Crossover} & \\
\mathbf{S}_0^{k_1} = \begin{bmatrix} 1 & 0 & 1 & 0 \\ 0 & 1 & 1 & 1 \\ 1 & 1 & 0 & 0 \end{bmatrix} & \mathbf{S}_1^{k_1} = \begin{bmatrix} 1 & 0 & 1 & 2 \\ 0 & 1 & 1 & 1 \\ 2 & 1 & 0 & 1 \end{bmatrix} \\
\mathbf{S}_0^{k_2} = \begin{bmatrix} 1 & 0 & 1 & 1 \\ 0 & 2 & 0 & 1 \\ 0 & 1 & 0 & 1 \end{bmatrix} & \mathbf{S}_1^{k_2} = \begin{bmatrix} 1 & 0 & 1 & 1 \\ 0 & 0 & 2 & 1 \\ 3 & 1 & 0 & 0 \end{bmatrix}
\end{array}$$

Fig. 13. Crossover example. The pair of offspring individuals are  $\Upsilon_{k_1} = \{\mathbf{S}_0^{k_1}, \mathbf{S}_1^{k_1}\}$  and  $\Upsilon_{k_2} = \{\mathbf{S}_0^{k_2}, \mathbf{S}_1^{k_2}\}$  ( $N_g < k_1 \neq k_2 \leq K$ ). Two selected positions are  $(u_1, v_1) = (2, 2)$  and  $(u_2, v_2) = (2, 3)$ . The entries in positions  $(2, 2)$ ,  $(3, 2)$ ,  $(1, 3)$ ,  $(2, 3)$  of  $\mathbf{S}_0^{k_1}$ , i.e.,  $[2 \ 1 \ 1 \ 0]$  are exchanged with those in the same positions of  $\mathbf{S}_0^{k_2}$ , i.e.,  $[1 \ 1 \ 1 \ 1]$ . Similarly,  $[0 \ 1 \ 1 \ 2]$  in  $\mathbf{S}_1^{k_1}$  are exchanged with  $[1 \ 1 \ 1 \ 1]$  in  $\mathbf{S}_1^{k_2}$ .

$$\begin{array}{cc}
\mathbf{S}_0^{k_1} = \begin{bmatrix} 1 & 0 & 1 & 0 \\ 0 & 1 & 1 & 1 \\ 1 & 1 & 0 & 0 \end{bmatrix} & \mathbf{S}_1^{k_1} = \begin{bmatrix} 1 & 0 & 1 & 2 \\ 0 & 1 & 1 & 1 \\ 2 & 1 & 0 & 1 \end{bmatrix} \\
\downarrow \text{Mutation} & \\
\mathbf{S}_0^{k_1} = \begin{bmatrix} 1 & 0 & 1 & 0 \\ 0 & 1 & 1 & 1 \\ 3 & 1 & 0 & 0 \end{bmatrix} & \mathbf{S}_1^{k_1} = \begin{bmatrix} 1 & 0 & 1 & 2 \\ 0 & 1 & 1 & 1 \\ 0 & 1 & 0 & 1 \end{bmatrix}
\end{array}$$

Fig. 14. Mutation example.  $\Upsilon_1 = \{\mathbf{S}_0^{k_1}, \mathbf{S}_1^{k_1}\}$  ( $N_g < k_1 \leq K$ ) and mutation occurs in all the  $(3, 1)$ -th entries. The entry 1 in  $\mathbf{S}_0^{k_1}$  is changed into 3 and the entry 2 in  $\mathbf{S}_1^{k_1}$  is changed into 0 to keep  $\mathbf{S}_0^{k_1} + \mathbf{S}_1^{k_1} = \mathbf{B}$  (30).

threshold and the corresponding SC-PLDPCH-CC has a good error performance at low  $E_b/N_0$ .

When GA is used to systematically search for optimal protomatrices, setting  $L = 10$  in the layered PEXIT algorithm can efficiently calculate the threshold of a SC-PLDPCH-TDC. Once the optimal protomatrices is found, we increase  $L$  so that the code rate of the SC-PLDPCH-TDC is very close to that of its SC-PLDPCH-CC. We further use the layered PEXIT method to

calculate the threshold of the lengthened SC-PLDPCH-TDC as proxy for the SC-PLDPCH-CC threshold.

#### IV. SIMULATION RESULTS

Based on the optimized PLDPCH-BCs found in [16], [17], we search for good SC-PLDPCH-CCs using the layered PEXIT algorithm and the GA proposed in Sect. III-D and Sect. III-E. We assume  $W = 1$ , and use  $L = 10$  and  $N_{\max} = 150$  in the layered PEXIT method. We also set  $K = 30$ ,  $N_g = 4$ ,  $p_c = 0.8$  and  $p_m = 0.6$  in the GA. We use binary phase-shift-keying (BPSK) modulation over an AWGN channel. Moreover, we apply the pipeline decoding with different number of processors to evaluate the error performance of the SC-PLDPCH-CCs found.

##### A. Rate-0.0494 and $r = 4$

Based on the  $7 \times 11$  protomatrix  $\mathbf{B}$  (shown in (25)) of the optimized rate-0.0494 PLDPCH-BC [16], [17], we apply GA and find two  $7 \times 11$  protomatrices, i.e.,

$$\mathbf{B}_0 = \begin{bmatrix} 1 & 0 & 0 & 0 & 0 & 0 & 1 & 0 & 1 & 0 & 0 \\ 0 & 0 & 1 & 0 & 0 & 0 & 0 & 0 & 0 & 2 & 1 \\ 2 & 1 & 0 & 0 & 0 & 0 & 0 & 0 & 0 & 0 & 1 \\ 0 & 1 & 0 & 1 & 0 & 0 & 0 & 0 & 0 & 2 & 0 \\ 1 & 0 & 0 & 0 & 0 & 0 & 0 & 1 & 0 & 1 & 0 \\ 1 & 0 & 0 & 2 & 0 & 0 & 0 & 0 & 0 & 0 & 0 \\ 1 & 0 & 0 & 0 & 1 & 0 & 0 & 0 & 0 & 2 & 0 \end{bmatrix} \quad (46)$$

and

$$\mathbf{B}_1 = \begin{bmatrix} 0 & 0 & 0 & 0 & 0 & 0 & 0 & 0 & 2 & 0 & 1 \\ 0 & 1 & 1 & 0 & 0 & 0 & 0 & 0 & 0 & 0 & 0 \\ 0 & 0 & 0 & 0 & 1 & 1 & 0 & 0 & 0 & 0 & 0 \\ 0 & 0 & 0 & 2 & 0 & 0 & 0 & 0 & 0 & 0 & 0 \\ 1 & 0 & 0 & 0 & 0 & 0 & 0 & 0 & 0 & 2 & 0 \\ 2 & 0 & 0 & 0 & 0 & 0 & 1 & 0 & 0 & 0 & 0 \\ 0 & 0 & 0 & 1 & 0 & 0 & 0 & 0 & 1 & 0 & 0 \end{bmatrix}, \quad (47)$$

after 13 generations. The corresponding fitness value equals 554. Then we increase  $L$  to 500 and the code rate of the SC-PLDPCH-TDC constructed by (46) and (47) is increased to about 0.0491, approaching that of underlying PLDPCH-BC [16], [17]. Using the proposed layered PEXIT method with  $N'_{\max} = 1000$  iterations, Table II lists the thresholds for the  $r = 4$  SC-



TABLE II  
 THRESHOLDS FOR  $r = 4$  SC-PLDPCH-TDC AND  $r = 4$  PLDPCH-BC [16], [17] COMPUTED BY THE PROPOSED PEXIT  
 ALGORITHM.  $N_{\max} = 1000$ .

Code	TDC	BC [16], [17]
Coupling width $W$	1	Not applicable
Coupling length $L$	500	Not applicable
Code rate $R$	0.0491	0.0494
Threshold in dB	-1.35	-1.34

PLDPCH-TDC with  $L = 500$ , and the  $r = 4$  PLDPCH-BC <sup>6</sup> [16], [17], respectively. The theoretical threshold of the terminated code with  $L = 500$  is found to be  $-1.35$  dB, which is approximated as the threshold of the SC-PLDPCH-CC constructed by (46) and (47). Note that the threshold is slightly lower than that of the PLDPCH-BC.

We use the lifting factors  $z_1 = 32$  and  $z_2 = 512$  to expand the protomatrix such that the sub-block length of the SC-PLDPCH-CC equals  $1,327,104$ , which is identical to the code length of the PLDPCH-BC with  $z_1 = 32$  and  $z_2 = 512$ , i.e.,  $N + M(2^r - r - 2) = 1,327,104$ . The BER performance of the SC-PLDPCH-CC with different number of processors  $I$  used in pipeline decoding is shown in Fig. 15. We observe that the decoder with  $I = 80$  processors in pipeline decoding achieves a BER of  $10^{-5}$  at about  $E_b/N_0 = -1.238$  dB, which outperforms that with  $I = 70$  by about 0.03 dB, and that with  $I = 60$  by about 0.06 dB. In the same figure, we also see that the SC-PLDPCH-CC outperforms the PLDPCH-BC using 300 standard decoding iterations (equivalent to 150 layered decoding iterations) by about 0.048 dB at a BER of  $10^{-5}$ . The gaps of the SC-PLDPCH-CC (with  $I = 80$  and BER of  $10^{-5}$ ) to the Shannon capacity ( $-1.44$  dB) of  $R = 0.05$  and to the ultimate Shannon limit ( $-1.59$  dB) are about 0.202 dB and 0.352 dB, respectively.

<sup>6</sup>In [16], [17], (37) has been used to compute  $I_{eh}$ . It is not very efficient because of the need to evaluate the PDF of the LLR values. In this paper, (38) is used instead to compute  $I_{eh}$  because it can be evaluated much more efficiently with graphics processing units. The computed thresholds are found to be slightly different and larger than those reported in [16], [17].

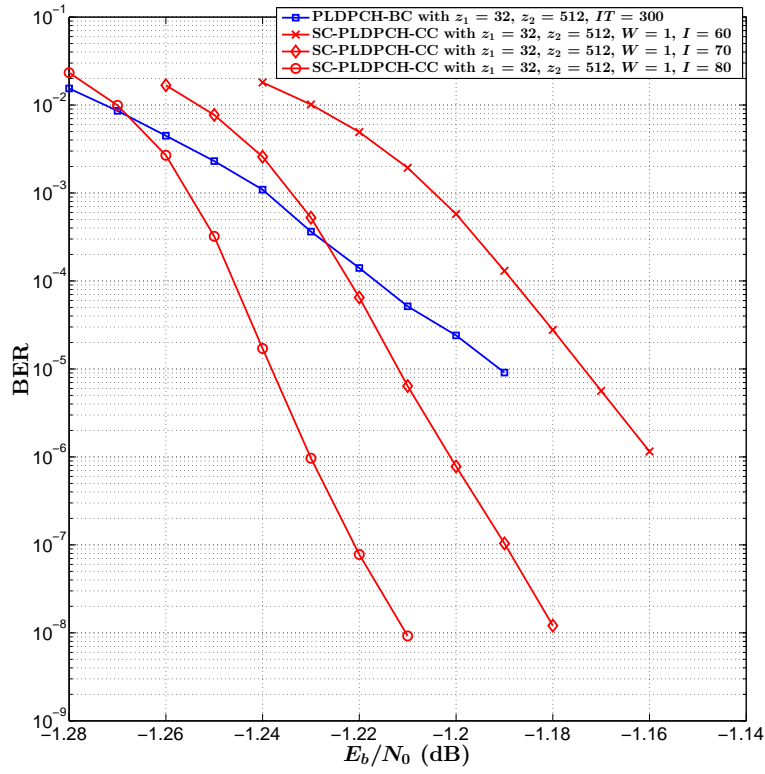


Fig. 15. BER performance comparison between the rate-0.0494 PLDPCH-BC and rate-0.0494 SC-PLDPCH-CC.  $r = 4$ .

### B. Rate-0.021 and $r = 5$

Based on the  $6 \times 10$  protomatrix

$$B = \begin{bmatrix} 3 & 2 & 0 & 0 & 1 & 0 & 0 & 0 & 1 & 0 \\ 0 & 0 & 2 & 0 & 0 & 2 & 1 & 2 & 0 & 0 \\ 0 & 0 & 0 & 3 & 1 & 0 & 0 & 1 & 0 & 2 \\ 0 & 1 & 0 & 1 & 0 & 0 & 0 & 2 & 0 & 3 \\ 0 & 0 & 0 & 2 & 0 & 0 & 1 & 2 & 0 & 2 \\ 2 & 0 & 1 & 1 & 0 & 0 & 0 & 2 & 0 & 1 \end{bmatrix} \quad (48)$$

TABLE III  
THRESHOLDS FOR  $r = 5$  SC-PLDPCH-TDC AND  $r = 5$  PLDPCH-BC [16], [17] COMPUTED BY THE PROPOSED PEXIT  
ALGORITHM.  $N_{\max} = 1000$ .

Code	TDC	BC [16], [17]
Coupling width $W$	1	Not applicable
Coupling length $L$	300	Not applicable
Code rate $R$	0.021	0.021
Threshold in dB	-1.37	-1.37

of the optimized rate-0.021 PLDPCH-BC [16], [17], we apply GA and find the following  $6 \times 10$  protomatrices

$$B_0 = \begin{bmatrix} 1 & 2 & 0 & 0 & 0 & 0 & 0 & 0 & 1 & 0 \\ 0 & 0 & 1 & 0 & 0 & 1 & 0 & 2 & 0 & 0 \\ 0 & 0 & 0 & 1 & 1 & 0 & 0 & 0 & 0 & 1 \\ 0 & 0 & 0 & 1 & 0 & 0 & 0 & 2 & 0 & 1 \\ 0 & 0 & 0 & 1 & 0 & 0 & 1 & 2 & 0 & 0 \\ 1 & 0 & 0 & 0 & 0 & 0 & 0 & 1 & 0 & 1 \end{bmatrix} \quad (49)$$

and

$$B_1 = \begin{bmatrix} 2 & 0 & 0 & 0 & 1 & 0 & 0 & 0 & 0 & 0 \\ 0 & 0 & 1 & 0 & 0 & 1 & 1 & 0 & 0 & 0 \\ 0 & 0 & 0 & 2 & 0 & 0 & 0 & 1 & 0 & 1 \\ 0 & 1 & 0 & 0 & 0 & 0 & 0 & 0 & 0 & 2 \\ 0 & 0 & 0 & 1 & 0 & 0 & 0 & 0 & 0 & 2 \\ 1 & 0 & 1 & 1 & 0 & 0 & 0 & 1 & 0 & 0 \end{bmatrix}, \quad (50)$$

after 50 generations. The corresponding fitness value equals 609. Using the proposed layered PEXIT method, Table III lists the thresholds for the  $r = 5$  SC-PLDPCH-TDC constructed by (49) and (50), and for the  $r = 5$  PLDPCH-BC [16], [17]. The theoretical threshold of the SC-PLDPCH-TDC with  $L = 300$  is estimated to be  $-1.37$  dB, which is the same with that of the PLDPCH-BC [16], [17]. Hence, we consider that the  $r = 5$  SC-PLDPCH-CC constructed by (49) and (50) has a threshold of about  $-1.37$  dB.

We use the same lifting factors, i.e.,  $z_1 = 32$  and  $z_2 = 512$ , as those used in the PLDPCH-BC to expand the protomatrix such that the sub-block length of the SC-PLDPCH-CC equals 3, 112, 960. The BER performance of the SC-PLDPCH-CC with different number of processors  $I$  is shown in Fig. 16. The pipeline decoder with  $I = 80$  processors achieves a BER of  $10^{-5}$  at about  $E_b/N_0 = -1.30$  dB, which outperforms that with  $I = 70$  by about 0.02 dB, and that with

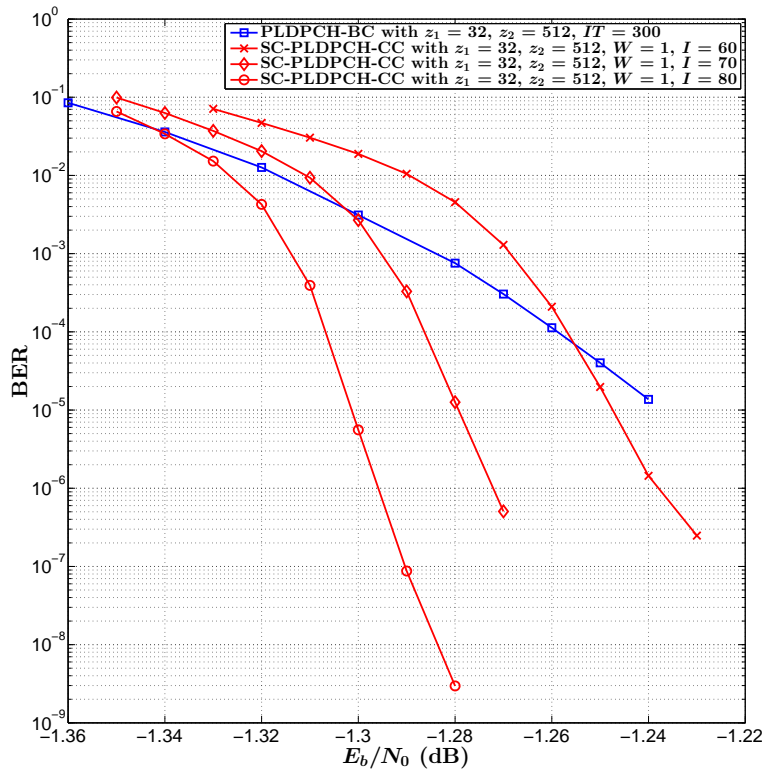


Fig. 16. BER performance comparison between the rate-0.021 PLDPCH-BC and rate-0.021 SC-PLDPCH-CC.  $r = 5$ .

$I = 60$  by about 0.05 dB. In the same figure, we also see that the SC-PLDPCH-CC outperforms the PLDPCH-BC using 300 standard decoding iterations by about 0.06 dB at a BER of  $10^{-5}$ . The gaps of the SC-PLDPCH-CC (with  $I = 80$  and BER of  $10^{-5}$ ) to the Shannon capacity ( $-1.53$  dB) of  $R = 0.02$  and to the ultimate Shannon limit ( $-1.59$  dB) are about 0.23 dB and 0.29 dB, respectively.

### C. Rate-0.008 and $r = 8$

The  $5 \times 15$  protomatrix  $\mathbf{B}$  of the optimized rate-0.008 PLDPCH-BC [16], [17], and the two protomatrices  $\mathbf{B}_0$  and  $\mathbf{B}_1$  obtained by our proposed GA are shown in (51), (52) and (53), respectively. The protomatrices (52) and (53) are found after 59 generations, and the corresponding fitness value equals 457.

TABLE IV  
 THRESHOLDS FOR  $r = 8$  SC-PLDPCH-TDC AND  $r = 8$  PLDPCH-BC [16], [17] COMPUTED BY THE PROPOSED PEXIT  
 ALGORITHM.  $N_{\max} = 1000$ .

Code	TDC	BC [16], [17]
Coupling width $W$	1	Not applicable
Coupling length $L$	300	Not applicable
Code rate $R$	0.008	0.008
Threshold in dB	-1.45	-1.44

$$\mathbf{B} = \begin{bmatrix} 2 & 0 & 1 & 0 & 0 & 0 & 0 & 3 & 2 & 0 & 0 & 1 & 0 & 0 & 1 \\ 0 & 2 & 0 & 1 & 1 & 0 & 0 & 0 & 0 & 0 & 0 & 3 & 0 & 3 & 0 \\ 0 & 0 & 1 & 0 & 0 & 2 & 2 & 0 & 0 & 1 & 1 & 2 & 1 & 0 & 0 \\ 0 & 0 & 0 & 2 & 2 & 0 & 0 & 0 & 0 & 1 & 0 & 3 & 0 & 0 & 2 \\ 0 & 0 & 0 & 0 & 0 & 1 & 1 & 0 & 1 & 1 & 1 & 2 & 3 & 0 & 0 \end{bmatrix} \quad (51)$$

$$\mathbf{B}_0 = \begin{bmatrix} 1 & 0 & 1 & 0 & 0 & 0 & 0 & 1 & 0 & 0 & 0 & 1 & 0 & 0 & 0 \\ 0 & 1 & 0 & 0 & 1 & 0 & 0 & 0 & 0 & 0 & 0 & 0 & 0 & 2 & 0 \\ 0 & 0 & 0 & 0 & 0 & 0 & 1 & 0 & 0 & 1 & 1 & 2 & 1 & 0 & 0 \\ 0 & 0 & 0 & 1 & 2 & 0 & 0 & 0 & 0 & 0 & 0 & 3 & 0 & 0 & 1 \\ 0 & 0 & 0 & 0 & 0 & 1 & 0 & 0 & 1 & 1 & 0 & 0 & 1 & 0 & 0 \end{bmatrix} \quad (52)$$

$$\mathbf{B}_1 = \begin{bmatrix} 1 & 0 & 0 & 0 & 0 & 0 & 0 & 2 & 2 & 0 & 0 & 0 & 0 & 0 & 1 \\ 0 & 1 & 0 & 1 & 0 & 0 & 0 & 0 & 0 & 0 & 0 & 3 & 0 & 1 & 0 \\ 0 & 0 & 1 & 0 & 0 & 2 & 1 & 0 & 0 & 0 & 0 & 0 & 0 & 0 & 0 \\ 0 & 0 & 0 & 1 & 0 & 0 & 0 & 0 & 0 & 1 & 0 & 0 & 0 & 0 & 1 \\ 0 & 0 & 0 & 0 & 0 & 0 & 1 & 0 & 0 & 0 & 1 & 2 & 2 & 0 & 0 \end{bmatrix} \quad (53)$$

We increase  $L$  to 300 such that the SC-PLDPCH-TDC has the same code rate with its underlying block code [16], [17]. Using our proposed PEXIT method, the terminated code with  $L = 300$  has a threshold of  $-1.45$  dB as shown in Table IV. Hence, the theoretical threshold of the SC-PLDPCH-CC constructed by (52) and (53) approximately equals  $-1.45$  dB, which is slightly lower than that of the PLDPCH-BC [16], [17].

We lift the SC-PLDPCH-CC with factors  $z_1 = 16$  and  $z_2 = 1280$  such that its sub-block length is the same as that of the PLDPCH-BC in [16], [17]. Fig. 17 shows the BER performance of the two codes. A SC-PLDPCH-CC pipeline decoder with  $I = 100$  processors achieves a BER of  $10^{-5}$  at about  $E_b/N_0 = -1.40$  dB, which outperforms that with  $I = 90$  by about 0.01 dB, and that with  $I = 80$  by about 0.025 dB. It outperforms the PLDPCH-BC using 300 standard

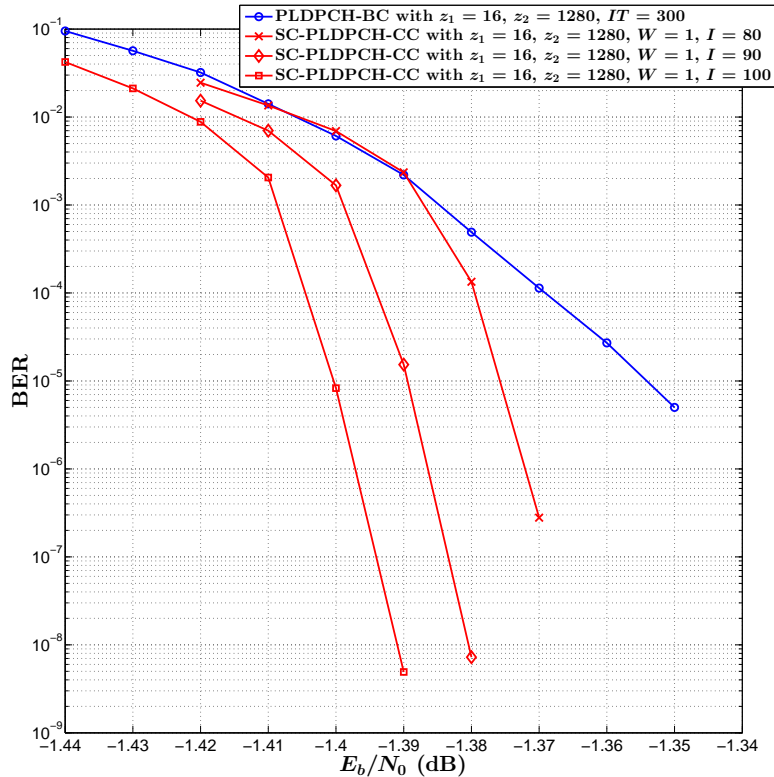


Fig. 17. BER performance comparison between the rate-0.008 PLDPCH-BC and rate-0.008 SC-PLDPCH-CC.  $r = 8$ .

TABLE V  
THRESHOLDS FOR  $r = 10$  SC-PLDPCH-TDC AND  $r = 10$  PLDPCH-BC [16], [17] COMPUTED BY THE PROPOSED PEXIT ALGORITHM.  $N_{\max} = 1000$ .

Code	TDC	BC [16], [17]
Coupling width $W$	1	Not applicable
Coupling length $L$	100	Not applicable
Code rate $R$	0.00291	0.00295
Threshold in dB	-1.48	-1.50

decoding iterations by about 0.05 dB at a BER of  $10^{-5}$ . At a BER of  $10^{-5}$ , the gaps (for the SC-PLDPCH-CC with  $I = 100$  iterations) to the Shannon capacity ( $-1.57$  dB) of  $R = 0.008$  and to the ultimate Shannon limit ( $-1.59$ ) dB are 0.17 dB and 0.19 dB, respectively.

$$\mathbf{B} = \begin{bmatrix} 1 & 0 & 0 & 0 & 0 & 0 & 3 & 0 & 0 & 0 & 0 & 0 & 0 & 0 & 2 & 0 & 0 & 0 & 0 & 1 & 4 & 0 & 1 & 0 \\ 0 & 0 & 0 & 3 & 2 & 0 & 0 & 0 & 1 & 1 & 0 & 0 & 1 & 0 & 0 & 0 & 3 & 1 & 0 & 0 & 0 & 0 & 0 & 0 \\ 0 & 1 & 2 & 0 & 0 & 1 & 0 & 0 & 0 & 0 & 0 & 0 & 0 & 0 & 1 & 0 & 0 & 3 & 0 & 4 & 0 & 0 & 0 \\ 0 & 0 & 0 & 0 & 0 & 0 & 0 & 1 & 0 & 0 & 3 & 3 & 0 & 0 & 0 & 0 & 0 & 0 & 0 & 2 & 2 & 0 & 1 \\ 2 & 2 & 0 & 0 & 0 & 0 & 0 & 0 & 0 & 0 & 0 & 0 & 1 & 0 & 1 & 0 & 1 & 0 & 3 & 0 & 0 & 1 & 1 \\ 0 & 0 & 0 & 0 & 0 & 1 & 0 & 3 & 3 & 2 & 0 & 0 & 1 & 1 & 0 & 0 & 0 & 0 & 0 & 1 & 0 & 0 & 0 \end{bmatrix} \quad (54)$$

$$\mathbf{B}_0 = \begin{bmatrix} 1 & 0 & 0 & 0 & 0 & 0 & 2 & 0 & 0 & 0 & 0 & 0 & 0 & 1 & 0 & 0 & 0 & 0 & 1 & 3 & 0 & 1 & 0 \\ 0 & 0 & 0 & 1 & 1 & 0 & 0 & 0 & 1 & 1 & 0 & 0 & 1 & 0 & 0 & 0 & 2 & 0 & 0 & 0 & 0 & 0 & 0 \\ 0 & 1 & 1 & 0 & 0 & 1 & 0 & 0 & 0 & 0 & 0 & 0 & 0 & 0 & 0 & 0 & 2 & 0 & 0 & 0 & 0 & 0 \\ 0 & 0 & 0 & 0 & 0 & 0 & 0 & 1 & 0 & 0 & 1 & 1 & 0 & 0 & 0 & 0 & 0 & 0 & 1 & 1 & 0 & 0 \\ 0 & 1 & 0 & 0 & 0 & 0 & 0 & 0 & 0 & 0 & 0 & 0 & 0 & 1 & 0 & 1 & 0 & 2 & 0 & 0 & 1 & 0 \\ 0 & 0 & 0 & 0 & 0 & 0 & 0 & 2 & 2 & 2 & 0 & 0 & 0 & 1 & 0 & 0 & 0 & 0 & 0 & 0 & 0 & 0 \end{bmatrix} \quad (55)$$

$$\mathbf{B}_1 = \begin{bmatrix} 0 & 0 & 0 & 0 & 0 & 0 & 1 & 0 & 0 & 0 & 0 & 0 & 0 & 1 & 0 & 0 & 0 & 0 & 1 & 0 & 0 & 0 \\ 0 & 0 & 0 & 2 & 1 & 0 & 0 & 0 & 0 & 0 & 0 & 0 & 0 & 1 & 1 & 0 & 0 & 0 & 0 & 0 & 0 & 0 \\ 0 & 0 & 1 & 0 & 0 & 0 & 0 & 0 & 0 & 0 & 0 & 0 & 0 & 1 & 0 & 0 & 1 & 0 & 4 & 0 & 0 & 0 \\ 0 & 0 & 0 & 0 & 0 & 0 & 0 & 0 & 0 & 2 & 2 & 0 & 0 & 0 & 0 & 0 & 0 & 0 & 1 & 1 & 0 & 1 \\ 2 & 1 & 0 & 0 & 0 & 0 & 0 & 0 & 0 & 0 & 0 & 0 & 1 & 0 & 0 & 0 & 0 & 1 & 0 & 0 & 0 & 1 \\ 0 & 0 & 0 & 0 & 0 & 1 & 0 & 1 & 1 & 0 & 0 & 0 & 1 & 0 & 0 & 0 & 0 & 0 & 1 & 0 & 0 & 0 \end{bmatrix} \quad (56)$$

#### D. Rate-0.00295 and $r = 10$

The  $6 \times 24$  protomatrix  $\mathbf{B}$  of the optimized rate-0.00295 PLDPCH-BC [16], [17], and the two protomatrices  $\mathbf{B}_0$  and  $\mathbf{B}_1$  obtained by our proposed GA are shown in (54), (55) and (56), respectively. The protomatrices (55) and (56) are found after 48 generations, and the corresponding fitness value equals 516. Using the proposed PEXIT method, Table IV lists the thresholds for SC-PLDPCH-TDC with  $L = 100$  and the underlying PLDPCH-BC [16], [17]. The SC-PLDPCH-TDC constructed by  $L = 100$  sets of protomatrices (55) and (56) has almost the same code rate with its underlying block code, and its threshold is estimated to be  $-1.48$  dB. Hence, the theoretical threshold of the SC-PLDPCH-CC constructed by (55) and (56) also equals  $-1.48$  dB, which is slightly greater than that of the PLDPCH-BC [16], [17].

We lift the SC-PLDPCH-CC with factors  $z_1 = 20$  and  $z_2 = 1280$  such that its sub-block length is the same as that of the PLDPCH-BC [16], [17]. Fig. 18 shows the BER performance of the two codes. SC-PLDPCH-CC decoder with  $I = 140$  processors achieves a BER of  $10^{-5}$  at about  $E_b/N_0 = -1.46$  dB, which outperforms that with  $I = 120$  by about 0.01 dB, and that with  $I = 100$  by about 0.03 dB. It outperforms the PLDPCH-BC using 300 standard decoding iterations by about 0.03 dB at a BER of  $10^{-5}$ . At a BER of  $10^{-5}$ , the gaps (for the SC-PLDPCH-CC with  $I = 140$  iterations) to the Shannon capacity ( $-1.58$  dB) of  $R = 0.003$  and to the ultimate Shannon limit ( $-1.59$ ) dB are 0.12 dB and 0.13 dB, respectively.

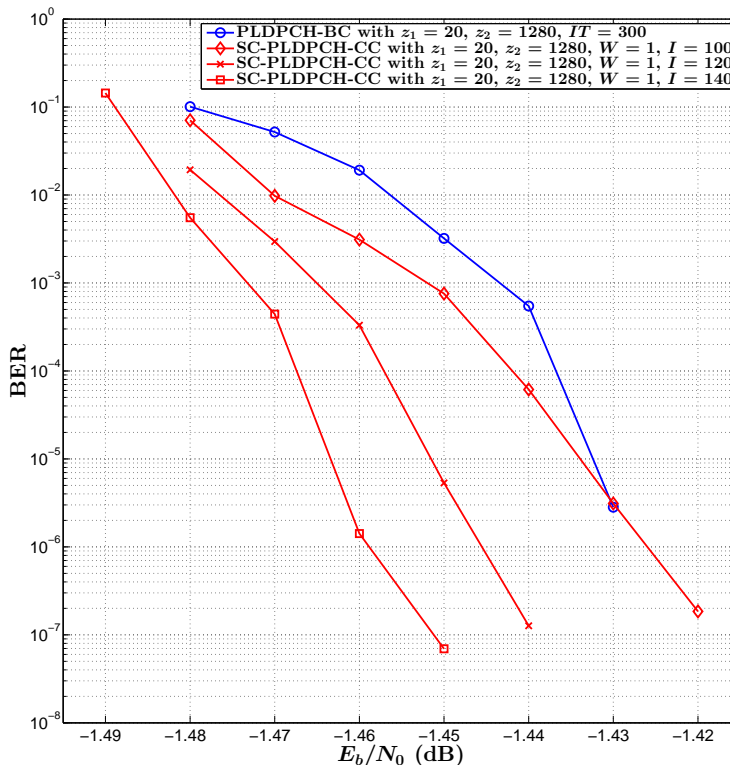


Fig. 18. BER performance comparison between the rate-0.00295 PLDPCH-BC and rate-0.00295 SC-PLDPCH-CC.  $r = 10$ .

## V. CONCLUSION

In this paper, we have proposed a new type of ultimate-Shannon-limit-approaching code called spatially coupled PLDPC-Hadamard convolutional codes (SC-PLDPCH-CCs). As the name implies, SC-PLDPCH-CCs are formed by spatially coupling PLDPC block codes (PLDPC-BCs). We have developed a pipelined decoding with layered scheduling algorithm to efficiently and effectively decode SC-PLDPCH-CCs. We have proposed a layered PEXIT method to evaluate the threshold of spatially coupled PLDPC-Hadamard terminated codes (SC-PLDPCH-TDCs) with an appropriate coupling length. Based on the protomatrix of a PLDPC-BC, we have proposed a genetic algorithm (GA) to systematically search for the protomatrices of good SC-PLDPCH-TDCs. We extend the coupling length of these SC-PLDPCH-TDCs with good thresholds to form SC-PLDPCH-CCs. Furthermore, we compute the lengthened SC-PLDPCH-TDC threshold as an estimation of the corresponding SC-PLDPCH-CC threshold.

Using the proposed methods, we have found SC-PLDPCH-CCs of rates 0.0494, 0.021, 0.008



and 0.00295. These SC-PLDPCH-CCs found are comparable to or superior to their block code counterparts in terms of theoretical threshold and error performance. Moreover, at a BER of  $10^{-5}$ , the SC-PLDPCH-CCs of rates 0.0494, 0.021, 0.008 and 0.00295 are only 0.352 dB, 0.29 dB, 0.19 dB and 0.13 dB from the ultimate Shannon limit, i.e.,  $-1.59$  dB. They are also the closest to ultimate Shannon limit in these four code rates compared with other published results.

## REFERENCES

- [1] R. G. Gallager, *Low-Density Parity-Check Codes*. PhD thesis, Cambridge, MA, USA, 1963.
- [2] R. M. Tanner, "A recursive approach to low complexity codes," *IEEE Trans. Inf. Theory*, vol. 27, no. 5, pp. 533–547, Sep. 1981.
- [3] T. J. Richardson, M. A. Shokrollahi, and R. L. Urbanke, "Design of capacity-approaching irregular low-density parity-check codes," *IEEE Trans. Inf. Theory*, vol. 47, no. 2, pp. 619–637, Feb. 2001.
- [4] S. T. Brink, G. Kramer, and A. Ashikhmin, "Design of low-density parity-check codes for modulation and detection," *IEEE Trans. Commun.*, vol. 52, no. 4, pp. 670–678, Apr. 2004.
- [5] E. Sharon, A. Ashikhmin, and S. Litsyn, "Analysis of low-density parity-check codes based on EXIT functions," *IEEE Trans. Commun.*, vol. 54, no. 8, pp. 1407–1414, 2006.
- [6] D. J. Costello and G. D. Forney, "Channel coding: The road to channel capacity," *Proc. IEEE*, vol. 95, no. 6, pp. 1150–1177, 2007.
- [7] L. Ping, L. Liu, K. Y. Wu, and W. K. Leung, "Approaching the capacity of multiple access channels using interleaved low-rate codes," *IEEE Commun. Lett.*, vol. 8, no. 1, pp. 4–6, 2004.
- [8] L. Ping, L. Liu, K. Wu, and W. Leung, "Interleave division multiple-access," *IEEE Trans. Wireless Commun.*, vol. 5, no. 4, pp. 938–947, 2006.
- [9] L. Ping, W. K. Leung, and K. Y. Wu, "Low-rate turbo-Hadamard codes," *IEEE Trans. Inf. Theory*, vol. 49, no. 12, pp. 3213–3224, Dec. 2003.
- [10] W. K. R. Leung, G. Yue, L. Ping, and X. Wang, "Concatenated zigzag Hadamard codes," *IEEE Trans. Inf. Theory*, vol. 52, no. 4, pp. 1711–1723, 2006.
- [11] S. Jiang, P. W. Zhang, F. C. M. Lau, C.-W. Sham, and K. Huang, "A turbo-Hadamard encoder/decoder system with hundreds of Mbps throughput," in *2018 IEEE 10th Int. Symp. Turbo Codes Iterative Inf. Process. (ISTC)*, pp. 1–5, 2018.
- [12] S. Jiang, P. W. Zhang, F. C. M. Lau, and C.-W. Sham, "An ultimate-shannon-limit-approaching Gbps throughput encoder/decoder system," *IEEE Trans. Circuits Syst. II, Exp. Briefs*, vol. 67, no. 10, pp. 2169–2173, 2020.
- [13] S. Jiang, F. C. M. Lau, and C.-W. Sham, "Hardware design of concatenated zigzag Hadamard encoder/decoder system with high throughput," *IEEE Access*, vol. 8, pp. 165298–165306, 2020.
- [14] G. Yue, L. Ping, and X. Wang, "Generalized low-density parity-check codes based on Hadamard constraints," *IEEE Trans. Inf. Theory*, vol. 53, no. 3, pp. 1058–1079, 2007.
- [15] X. Y. Hu, E. Eleftheriou, and D. M. Arnold, "Regular and irregular progressive edge-growth Tanner graphs," *IEEE Trans. Inf. Theory*, vol. 51, no. 1, pp. 386–398, Jan. 2005.
- [16] P. W. Zhang, F. C. M. Lau, and C.-W. Sham, "Protograph-based low-density parity-check Hadamard codes," *arXiv:2010.08285*, 2021.
- [17] P.-W. Zhang, F. C. M. Lau, and C.-W. Sham, "Protograph-based LDPC Hadamard codes," *IEEE Trans. Commun.*, vol. 69, no. 8, pp. 4998–5013, 2021.

- [18] J. Thorpe, “Low-density parity-check (LDPC) codes constructed from protographs,” in *Proc. IPN Progr. Rep.*, pp. 1–7, Aug. 2003.
- [19] M. Fossorier, “Quasi-cyclic low-density parity-check codes from circulant permutation matrices,” *IEEE Trans. Inf. Theory*, vol. 50, no. 8, pp. 1788–1793, Aug. 2004.
- [20] G. Liva and M. Chiani, “Protograph LDPC codes design based on EXIT analysis,” *IEEE GLOBECOM 2007*, pp. 3250–3254, 2007.
- [21] P. W. Zhang, F. C. M. Lau, and C.-W. Sham, “Layered decoding for protograph-based low-density parity-check Hadamard codes,” *IEEE Commun. Lett.*, vol. 25, no. 6, pp. 1776–1780, 2021.
- [22] A. R. Iyengar, M. Papaleo, P. H. Siegel, J. K. Wolf, A. Vanelli-Coralli, and G. E. Corazza, “Windowed decoding of protograph-based LDPC convolutional codes over erasure channels,” *IEEE Trans. Inf. Theory*, vol. 58, no. 4, pp. 2303–2320, 2012.
- [23] A. Jimenez Felstrom and K. Zigangirov, “Time-varying periodic convolutional codes with low-density parity-check matrix,” *IEEE Trans. Inf. Theory*, vol. 45, no. 6, pp. 2181–2191, 1999.
- [24] S. Kudekar, T. J. Richardson, and R. L. Urbanke, “Threshold saturation via spatial coupling: Why convolutional LDPC ensembles perform so well over the BEC,” *IEEE Trans. Inf. Theory*, vol. 57, no. 2, pp. 803–834, 2011.
- [25] S. Kudekar, T. Richardson, and R. L. Urbanke, “Spatially coupled ensembles universally achieve capacity under belief propagation,” *IEEE Trans. Inf. Theory*, vol. 59, no. 12, pp. 7761–7813, 2013.
- [26] M. Stinner and P. M. Olmos, “On the waterfall performance of finite-length SC-LDPC codes constructed from protographs,” *IEEE J. Sel. Areas Commun.*, vol. 34, no. 2, pp. 345–361, 2016.
- [27] M. Srinivas and L. M. Patnaik, “Genetic algorithms: A survey,” *Computer*, vol. 27, no. 6, pp. 17–26, 1994.
- [28] L. Hebbes, R. Malyan, and A. Lenaghan, “Genetic algorithms for turbo codes,” in *Proc. The Int. Conf. “Computer as a Tool”*, vol. 1, pp. 478–481, 2005.
- [29] A. Elkelesh, M. Ebada, S. Cammerer, and S. T. Brink, “Decoder-tailored polar code design using the genetic algorithm,” *IEEE Trans. Commun.*, vol. 67, no. 7, pp. 4521–4534, 2019.
- [30] A. Elkelesh, M. Ebada, S. Cammerer, L. Schmalen, and S. T. Brink, “Decoder-in-the-loop: Genetic optimization-based LDPC code design,” *IEEE Access*, vol. 7, pp. 141161–141170, 2019.
- [31] Y. Koganei, M. Yofune, C. Li, T. Hoshida, and Y. Amezawa, “SC-LDPC code with nonuniform degree distribution optimized by using genetic algorithm,” *IEEE Commun. Lett.*, vol. 20, no. 5, pp. 874–877, 2016.
- [32] Y. Wang, S. C. Draper, and J. S. Yedidia, “Hierarchical and high-girth QC LDPC codes,” *IEEE Trans. Inf. Theory*, vol. 59, no. 7, pp. 4553–4583, 2013.
- [33] D. J. Costello, L. Dolecek, T. E. Fuja, J. Kliewer, D. G. Mitchell, and R. Smarandache, “Spatially coupled sparse codes on graphs: Theory and practice,” *IEEE Commun. Mag.*, vol. 52, no. 7, pp. 168–176, 2014.
- [34] C.-W. Sham, X. Chen, F. C. M. Lau, Y. Zhao, and W. M. Tam, “A 2.0 Gb/s throughput decoder for QC-LDPC convolutional codes,” *IEEE Trans. Circuits Syst. I, Reg. Papers*, vol. 60, no. 7, pp. 1857–1869, 2013.
- [35] Y. Fang, G. A. Bi, Y. L. Guan, and F. C. M. Lau, “A survey on protograph LDPC codes and their applications,” *IEEE Commun. Surv. Tut.*, vol. 17, no. 4, pp. 1989–2016, 2015.
- [36] S. T. Brink, “Convergence behavior of iteratively decoded parallel concatenated codes,” *IEEE Trans. Commun.*, vol. 49, no. 10, pp. 1727–1737, Oct. 2001.
- [37] Z. Yang, Y. Fang, G. Cai, G. Zhang, and P. Chen, “Design and optimization of tail-biting spatially coupled protograph LDPC codes under shuffled belief-propagation decoding,” *IEEE Commun. Lett.*, vol. 24, no. 7, pp. 1378–1382, 2020.
- [38] J. H. Holland, *Adaptation in Natural and Artificial System*. Univ. of Michigan Press, Ann Arbor, 1975.